Separating chemistry and transport effects in two-dimensional models

Debra K. Weisenstein, Janusz Eluszkiewicz, Malcolm K. W. Ko,[1] and Courtney J. Scott
Atmospheric and Environmental Research, Lexington, Massachusetts, USA

Charles H. Jackman, Eric L. Fleming,[2] and David B. Considine[1]
NASA Goddard Space Flight Center, Greenbelt, Maryland, USA

Douglas E. Kinnison,[3] Peter S. Connell, and Douglas A. Rotman
Lawrence Livermore National Laboratory, Livermore, California, USA

Received 8 March 2004; revised 29 May 2004; accepted 21 June 2004; published 29 September 2004.

[1] Representation of transport in numerical models is known to be a major uncertainty in modeling of the atmosphere. Models also differ in their treatment of gas phase and heterogeneous chemistry. This paper will describe a quantitative approach to diagnosing the source of intermodel differences in ozone assessment calculations. Our approach is applied to diagnosing the differences between two-dimensional (2-D) models from Atmospheric and Environmental Research, the NASA Goddard Space Flight Center, and the Lawrence Livermore National Laboratory. Surprisingly, we find that differences due to chemical formulation are often as large as those due to transport, despite the fact that all models use the same set of reaction rate coefficients. These differences are particularly large when polar stratospheric cloud (PSC) processes are included in the models, though differences due to photolysis rates and details of the sulfate chemistry are also apparent. Perturbation calculations for a scenario including supersonic commercial aircraft operating in the 2015 stratosphere reveal that differences in the accumulation of H_2O and NO_y emitted by aircraft are due almost entirely to transport, while differences in ozone due to chemical formulation are evident in the lower stratosphere even without differences in H_2O and NO_y and without PSCs. By demonstrating a capability of separating transport and chemical differences, it is hoped that the results described in this paper will stimulate analogous studies with other models and will thus lead to a deeper understanding of intermodel similarities and differences, along with a means to quantify uncertainties in model predictions of atmospheric response to perturbations. *INDEX TERMS:* 0341 Atmospheric Composition and Structure: Middle atmosphere—constituent transport and chemistry (3334); 3337 Meteorology and Atmospheric Dynamics: Numerical modeling and data assimilation; 3334 Meteorology and Atmospheric Dynamics: Middle atmosphere dynamics (0341, 0342); *KEYWORDS:* modeling, stratosphere, aircraft

Citation: Weisenstein, D. K., J. Eluszkiewicz, M. K. W. Ko, C. J. Scott, C. H. Jackman, E. L. Fleming, D. B. Considine, D. E. Kinnison, P. S. Connell, and D. A. Rotman (2004), Separating chemistry and transport effects in two-dimensional models, *J. Geophys. Res.*, *109*, D18310, doi:10.1029/2004JD004744.

1. Introduction

[2] Studies have shown that the representation of transport is a major uncertainty in 2-D and 3-D modeling of the atmosphere [*Jackman et al.*, 1991; *Kinnison et al.*, 1994a; *Douglass et al.*, 1999]. Models also differ in their treatment of chemistry. Though most models employ the chemical reaction rates from JPL [*DeMore et al.*, 1997; *Sander et al.*, 2000], differences exist in family groupings, numerical techniques, diurnal averaging technique, and treatment of heterogeneous chemistry. Calculations of ozone perturbations by different models show differences that are not easy to interpret. How much of these differences are due to differences in transport? How much to differences in chemistry? Better understanding of intermodel differences would help in placing uncertainty estimates around model predictions of future ozone changes.

[3] Model intercomparisons have typically involved comparisons of spatial and temporal distributions of trace gases. The latitude-time distribution of column ozone is a

[1] Now at NASA Langley Research Center, Hampton, Virginia, USA.
[2] Also at Science Systems and Applications, Inc., Lanham, Maryland, USA.
[3] Now at National Center for Atmospheric Research, Boulder, Colorado, USA.

0148-0227/04/2004JD004744$09.00

common metric. Information on differences in chemistry is obtained by comparing radical concentrations calculated using specified long-lived species concentrations (see, e.g., the chemistry intercomparisons reported in Models and Measurements (M&M) I [*Prather and Remsberg*, 1993] and M&M II [*Park et al.*, 1999]). Intercomparisons of model transport use distributions of idealized tracers calculated with prescribed production and loss rates. Tracer concentrations are then compared, or quantities such as age of air are derived from the tracer mixing ratios [*Hall et al.*, 1999; *Park et al.*, 1999].

[4] This paper will describe a more quantitative approach to diagnosing the source of intermodel differences and apply it to three two-dimensional (2-D) models developed at Atmospheric and Environmental Research (AER), the Goddard Space Flight Center (GSFC), and the Lawrence Livermore National Laboratory (LLNL). In this approach, the chemical formulation of the AER model has been combined with the transport parameters (wind fields, diffusion coefficients) and numerical solution technique (grid resolution, advection scheme, and integration technique) of the LLNL and GSFC models to construct hybrid AER/GSFC and AER/LLNL models. The hybrid models allow chemical differences for both long- and short-lived species to be evaluated by comparing two models with the same transport but different chemical formulations (e.g., the hybrid AER/GSFC and the native GSFC model). The effect of transport on model-calculated perturbations can be evaluated by comparing results from the native AER model with the results from the hybrid models. This modular approach to model intercomparison has been used in the 3-D Global Modeling Initiative (GMI) model [*Douglass et al.*, 1999; *Considine et al.*, 2000; *Rotman et al.*, 2001; *Kinnison et al.*, 2001].

[5] It should be noted that the results presented in this paper have been generated by the circa 1997 versions of the models used in the M&M II report [*Park et al.*, 1999] and in the International Panel on Climate Change report on Aviation and the Global Atmosphere [*Intergovernmental Panel on Climate Change* (*IPCC*), 1999]. While each model has undergone further development since then, we believe that an in-depth comparison of these three models in their 1997 versions will provide important insights into intermodel differences evident (but not always explained) in those highly publicized reports. Moreover, some of these insights have stimulated important modifications to the participating models and thus their detailed description will provide a reference for both ongoing and future work with these models. By demonstrating a capability of separating transport and chemical differences, it is hoped that the results described in this paper will stimulate analogous studies with other models and thus lead to a deeper understanding of intermodel similarities and differences and their impacts on model predictions.

[6] The organization of this paper is as follows. Section 2 describes the dynamical and chemical formulations of the three models, followed by a description of our intercomparison approach in section 3. Section 4 intercompares simulations for the background atmosphere as projected to 2015, while section 5 presents an intercomparison of calculated perturbations to H_2O, NO_y, and ozone due to a future fleet of stratospheric aircraft. A discussion of the results and conclusions are presented in section 6.

2. Model Descriptions

[7] The three models considered here differ substantially in their formulations, including details of chemistry and dynamics. All three models use log pressure as the vertical coordinate, but vertical resolution varies from 1.2 km in the AER model to 1.5 km in the LLNL model to 2.0 km in the GSFC model. The GSFC model uses 10 degree horizontal resolution, the AER model 9.5 degree horizontal resolution, and the LLNL model 5 degree horizontal resolution. The GSFC model extends to 90 km, the LLNL model to 80 km, and the AER model only to 60 km. All three models use observed climatological temperatures taken from NCEP analyses [*Kalnay et al.*, 1996] to determine temperature-dependent reaction rates and, for the AER and GSFC models, to calculate polar stratospheric cloud surface area density. Our purpose here is not to justify the parameterizations and choices made by each modeling group, but to compare the models under controlled conditions to understand how model differences impact ozone perturbation calculations. On the basis of theoretical considerations, we believe that the GSFC model has the most realistic transport formulation, but with a simplified chemical formulation (due to lack of diurnal calculations for all species). The AER and LLNL models both perform explicit diurnal calculations for all species, so should yield similar chemical solutions, though their approaches are very different. AER's chemical formulation is more efficient with accuracy dependent on the chosen time step, while LLNL uses the more precise SMVGEARII chemistry operator [*Jacobson*, 1995].

2.1. Transport Parameters

[8] The transport parameters (i.e., horizontal and vertical wind fields, horizontal and vertical diffusion parameters) of the LLNL model [*Kinnison et al.*, 1994b; *Li et al.*, 1995] are computed using model-calculated ozone and observed temperatures. Mechanical forcing from planetary wave breaking (represented explicitly by two waves), gravity wave breaking, and Rayleigh friction are also employed. While this calculation is done interactively in the original LLNL model, the transport parameters from a previous calculation have been saved and used repeatedly in the LLNL results and the hybrid model calculations presented here. The horizontal diffusion K_{yy} is calculated as the ratio of the E-P flux divergence to the gradient of potential vorticity [*Garcia*, 1991], with a minimum value set at 1×10^8 cm^2/s in the stratosphere. Figures 1a and 1b show vertical velocity and K_{yy} from the LLNL model for October. Note the large gradients in the K_{yy} fields, from background levels of 1×10^8 cm^2/s over large areas to 3×10^{10} cm^2/s in the subtropical surf zones in October, and up to 4×10^{11} cm^2/s in the December surf zones. Tropospheric K_{yy} is set to 1×10^{10} cm^2/s. A gravity wave breaking parameterization is used to calculate K_{zz} in the stratosphere, with values ranging from 2×10^3 cm^2/s to over 1×10^5 cm^2/s. K_{zz} in the troposphere is set to 4×10^4 cm^2/s. The *Smolarkiewicz* [1984] scheme is used for advection in the LLNL model.

[9] The GSFC model [*Jackman et al.*, 1996; *Fleming et al.*, 1999] calculates transport parameters from observed

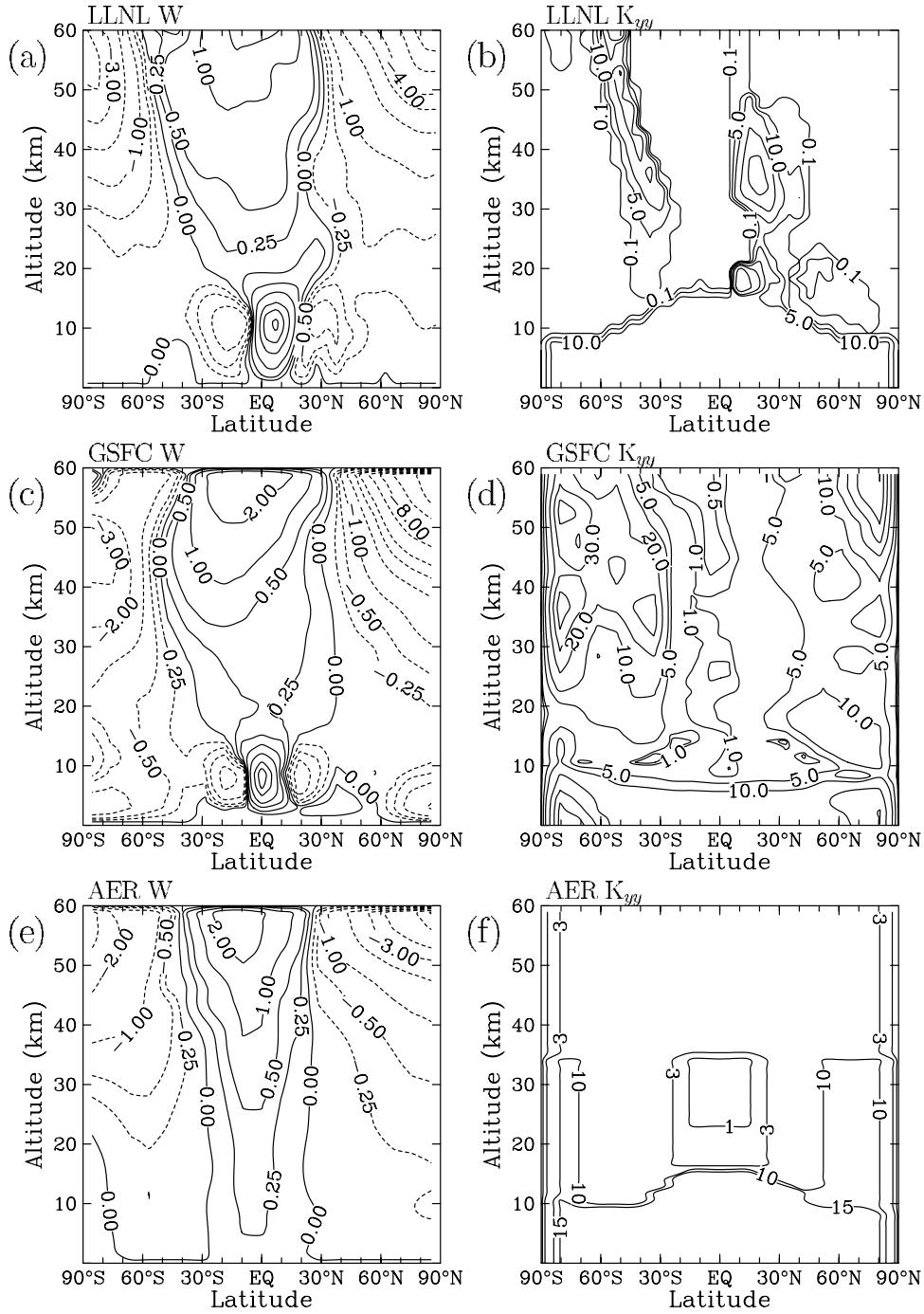

Figure 1. Model values of vertical velocity (in millimeters per second) and K_{yy} (in 10^9 cm^2/s) in October from (a and b) the LLNL model, (c and d) the GSFC model, and (e and f) the AER model.

climatological values of temperature, H_2O, zonal wind, and ozone. Mechanical forcing from six planetary waves (constructed from the observed temperature field) and effects of gravity wave breaking provide the wave driving. The diabatic heating rates are computed following *Rosenfield et al.* [1994], with the latent heating in the troposphere taken from *Newell et al.* [1974]. The stream function is obtained by solving an elliptic equation obtained by combining the zonal mean momentum and energy equations [see, e.g., *Garcia and Solomon*, 1983]. Figure 1c shows vertical velocity for October from the GSFC model. K_{yy} is computed using a similar theoretical basis as that used by the LLNL model but employing observed meteorological data and following the approach of *Randel and Garcia* [1994]. K_{yy} values range from 1×10^8 to 5×10^{10} cm^2/s, with values computed in both troposphere and stratosphere. Figure 1d shows K_{yy} values for October from the GSFC model. Maximum stratospheric K_{yy} values occur near 30–40°S coincident with the subtropical surf zone, and at high latitudes near 80°S coincident with the onset of the spring breakup of the polar vortex. K_{zz} values in the troposphere and lower stratosphere are based on the vertical temperature

gradients. In the upper stratosphere and mesosphere, K_{zz} values are obtained from a gravity wave parameterization, based on that originally developed by *Lindzen* [1981] and modified by *Holton and Zhu* [1984]. Stratospheric values of K_{zz} range from 1×10^2 cm^2/s in the lowermost stratosphere to 5×10^5 cm^2/s in the upper stratosphere. Tropospheric values of K_{zz} range from 1×10^4 cm^2/s at the tropopause to 5×10^5 cm^2/s at the surface in the tropics and 2.5×10^5 cm^2/s at the surface near the poles. The monotonic version of the Lin and Rood scheme [*Lin and Rood*, 1996] is used for advective transport in the GSFC model.

[10] The AER model uses transport parameters obtained in a more ad hoc manner than the GSFC or LLNL models. Heating rates, based loosely on *Dopplick* [1979], are scaled by temperature lapse rate to obtain the vertical velocity. The vertical velocity field is integrated to obtain a stream function, with adjustments made to assure mass conservation [see *Ko et al.*, 1985]. Diffusion rates are specified independently of the advective circulation, with K_{yy} values in the lower stratosphere based on studies of exchange timescales between the tropics and midlatitudes [*Shia et al.*, 1998]. Values chosen are from $0.7-1.3 \times 10^9$ cm^2/s in the tropics and from $3-10 \times 10^9$ cm^2/s elsewhere. K_{zz} values are constant at 1×10^5 cm^2/s in the troposphere, 1×10^3 cm^2/s in the lower and middle stratosphere, and 1×10^4 cm^2/s in the upper stratosphere. K_{yz} values are obtained by projecting the K_{yy} values from isentropic surfaces to pressure surfaces. There has been no attempt to maintain consistency between the advective and diffusive components of transport within the AER model. Figures 1e and 1f show vertical velocity and K_{yy} for October from the AER model. The parameterized K_{yy} values shown are constant for six months of the year, changing in April and October. The *Smolarkiewicz* [1984] scheme is used for advection in the AER model.

[11] The LLNL and GSFC models show strong Hadley circulations in the troposphere, while the AER model has none. The AER circulation is the weakest overall in the stratosphere, while the AER diffusion coefficients are the largest. Mean age of air calculated from the models reflects both advective and diffusive transport and can be compared with age fields derived from observations. As reported in the M&M II report [*Park et al.*, 1999], the GSFC model has the oldest age of air in the upper high latitude stratosphere at 4 years, the LLNL age is about 3.5 years, and the AER age about 3 years. All 2-D models and most 3-D models generate ages of air younger than observations indicate (5–7 years or more [*Park et al.*, 1999]), thus none can be regarded as truly representative of the complexities of transport in the real atmosphere.

2.2. Diurnal Treatment and Time Stepping Scheme

[12] Approaches to time stepping and diurnal variability differ significantly among the three models. The AER and GSFC models use a family approach and transport only long-lived species, whereas the LLNL model does explicit time stepping of all species. The GSFC model transports the species N_2O_5 and $ClONO_2$ which the AER model considers part of the NO_y and/or Cl_y families. Since zonal mean quantities are transported in 2-D models, zonally averaged production and loss rates are used in the continuity equation for long-lived species, with different techniques employed to obtain the zonal mean production and loss rates. These involve first calculating the diurnal variations in the radical species.

[13] The LLNL model calculates explicit diurnal chemistry for all species. Time marching is performed for 2 days at a time, alternately advancing the chemistry with 15-min time steps and the transport with 2-hour time steps. The chemistry operator performs integration with SMVGEARII, a grouped stiffness-ordered, sparse matrix implementation of the variable internal time step, variable order, implicit error-controlled Gear solution technique [*Jacobson*, 1995]. To save computer time, the diurnal version is run for one year while saving diurnal averaging coefficients daily. Then the diurnal average version of the model is run for two years using these coefficients until annually repeating conditions are obtained.

[14] The GSFC model performs explicit diurnal calculations only for those species that are produced at night, i.e., HNO_3, NO_2, NO_3, N_2O_5, HOCl, HCl, ClO, $ClONO_2$, BrO, HOBr, and $BrONO_2$. For other species, daytime average photolysis rates are used, along with dawn values of the night species, to calculate daytime average radical concentrations and production and loss rates for long-lived species. Time stepping of long-lived species is done with split operators, using a 12-hour time step for advection, a 3-hour step for vertical diffusion, a 24-hour step for horizontal diffusion, and a 24-hour step for chemistry.

[15] Computation of radical species in the AER model is performed with 17 explicit time steps over the diurnal cycle. Production and loss rates of long-lived species are computed from the radical concentrations at each of the 17 time steps and averaged over 24 hours. New production and loss rates are computed daily. The rates of change due to chemistry, diffusion, and advection are used to update long-lived species with a time step of 6 hours using an explicit scheme.

2.3. Chemistry Content

[16] Each model uses the JPL-97 compendium [*DeMore et al.*, 1997] as the source of reaction rate data. The monthly mean zonal mean temperature from climatology is used to calculate the rate constants for gas phase reactions. Six heterogeneous reactions on sulfate aerosol are employed in each model. Aerosol surface area is specified in these calculations, so reaction rates on sulfate aerosol are the same for all three models except for the way temperature variation is included in the rate calculation. Both LLNL and AER utilize a temperature probability distribution taken from NCEP reanalysis data [*Kalnay et al.*, 1996] which accounts for longitudinal and day-by-day deviations of temperature from the monthly zonal mean temperature. The reaction probability and the molecular thermal velocity are evaluated at each temperature in the distribution and then the mean value of the product is used, along with the aerosol surface area, to obtain the zonal mean reaction rate. This methodology is found to make a significant difference in reaction rates for those reactions which are strongly temperature-dependent ($ClONO_2 + H_2O$, $BrONO_2 + H_2O$, $ClONO_2 + HCl$) [*Weisenstein et al.*, 1998; *Pitari*, 1993]. The GSFC model employs only the zonal mean temperature in the rate calculation for sulfate aerosols.

[17] Various intercomparison exercises have demonstrated that standard application of Beer's law to account for O_2 and O_3 absorption in photolysis calculations provides reliable results in most cases. Care must be used, however, in the

Schumann-Runge (S-R) bands for O_2 photolysis and NO absorption. Models differ in the spectral resolution of their photolysis codes and the wavelength range considered.

[18] The AER model uses the photolysis code of *Prather* [1993] which handles the S-R bands according to *Minschwaner et al.* [1992]. The online photolysis calculation includes the effects of Rayleigh scattering in a spherical atmosphere. The attenuated flux in 77 wavelength bands at each grid point is calculated and multiplied by the molecular cross sections obtained from *DeMore et al.* [1997]. Photolysis rates or J rates are the integral of this product over wavelength, and are calculated for the ten daytime time points. Photolysis rates for O_2 and NO are calculated separately to account for the fine structure of the S-R bands.

[19] The GSFC and LLNL models use a lookup table for the photolytic source term (PST) which provides normalized attenuated solar flux as a function of pressure, wavelength, solar zenith angle, and column ozone. The table was generated by R. Kawa (GSFC) using a radiation code developed by D. Anderson and coworkers at the Johns Hopkins University Applied Physics Laboratory [*Anderson and Meier*, 1979; *Anderson and Lloyd*, 1990]. Molecular cross sections for photolysis are taken from laboratory measurements [*DeMore et al.*, 1997]. The J values are then determined online by integrating, over wavelength, the product of the exoatmospheric flux, the interpolated PST, and the molecular cross section at the local temperature. Because evaluation of $J(O_2)$ requires treatment of the S-R bands, a separate look-up table is employed for $J(O_2)$.

[20] All three models include lightning as a source of NO_y in the tropical troposphere, with the AER and GSFC models assuming a source strength of 2 megatons per year distributed from 4 to 14 km in altitude. The LLNL model assumes a source strength of 5 megatons per year distributed according to the ISCCP cloud database [*Rossow and Schiffer*, 1999]. Some species are removed in the troposphere through rainout/washout processes in each of the models, though both the rates of these processes and the species subject to washout vary somewhat from model to model. Washout rates in the LLNL model vary from 3 days in the lowest 4 km to 50 days near the tropopause. The AER model uses similar washout rates (5 days near the surface to 40 days at 10 km), but with no washout above 10 km. The GSFC model used the slowest washout rates: from 25 to 100 days.

[21] Distributions of H_2O in the troposphere are based on prescribed relative humidity values in the AER and LLNL models. In addition, the AER model specifies the water vapor mixing ratio just above the tropopause (2.75 ppmv in the tropics, up to 3.5 ppmv at high latitudes). The GSFC model sets water vapor at the bottom two model levels (879 and 661 mb) to the climatology of *Oort* [1983]. Water vapor is transported at higher levels in the troposphere in the GSFC model, with H_2O concentrations in excess of a specified relative humidity removed up to the prescribed daily and latitudinally varying tropopause level [*Fleming et al.*, 1995]. All three models calculate H_2O concentrations in the stratosphere and mesosphere using appropriate chemical sources (including methane oxidation) and sinks.

2.4. Polar Heterogeneous Chemistry Formulation

[22] While gas phase reaction rates of stratospheric interest have been fairly well standardized by the JPL compendium [*DeMore et al.*, 1997], treatment of heterogeneous chemistry, particularly under cold polar conditions, differs greatly between models. Differences concern assumptions about the composition of type I polar stratospheric cloud (PSC) particles, with possible choices of nitric acid trihydrate (NAT), sulfuric acid trihydrate (SAT), or supercooled ternary solution (STS). Furthermore, some models calculate PSC surface area based on model-calculated HNO_3 and H_2O, while others base PSC surface area on observations. In addition, different models employ different techniques to account for zonal asymmetries in temperature. Since there is no consensus on how to best represent cold polar processes, the GSFC, LLNL, and AER models implement different approaches.

[23] Both GSFC and AER employ thermodynamic equilibrium parameterizations to calculate type I (assumed to be NAT) and type II (ice) PSCs based on available gas phase H_2O and HNO_3 and a distribution of temperatures. The GSFC model assumes that supersaturation factors of 10 for NAT and 1.4 for ice are required before PSCs form. The AER model assumes no supersaturation. The GSFC model assumes lognormal size distributions of PSC particles, with NAT having a mode radius of 1.0 μm and a σ of 1.8 and ice particles having a mode radius of 10 μm and a σ of 1.8 [*Considine et al.*, 1994]. The AER model assumes a single radius for each type of particle, 0.5 μm for NAT and 7 μm for ice. Because of the particle size assumptions, the GSFC model has greater sedimentation and denitrification. In the GSFC model, the temperature probability distributions used to account for zonal temperature variability are only used to calculate surface area, and the zonal mean temperatures are used to calculated the heterogeneous reaction rates. In the AER model, temperature probability distribution functions are used to obtain the product of the reaction rate and surface area.

[24] The LLNL model handles cold heterogeneous processes by assigning a supercooled ternary solution (STS) composition to PSC particles. The particle surface area is not calculated by the model. Instead, a surface area density of 1 $\mu m^2/cm^3$ is imposed within 25° of the poles when the PSC climatology of *Poole and Pitts* [1994] indicates a PSC frequency of occurrence exceeding 0.08. Reaction rates are obtained by integrating over the temperature distribution and then multiplying by the fixed PSC surface area. Dehydration and denitrification are represented globally (independent of the PSC surface area parameterization) by assuming that the partial pressure in excess of the saturation vapor pressure over ice (calculated using zonal mean temperatures) is removed permanently with first-order time constants of 1 day for H_2O and 0.5 days for HNO_3.

3. Intercomparison Approach

3.1. Hybrid Models

[25] The heart of our intercomparison approach consists of two hybrid models referred to as the AER/GSFC and AER/LLNL models. Both hybrid models employ the AER chemistry formulation (including the photolysis scheme, reaction rates, heterogeneous chemistry for sulfate and PSCs, family approach, and diurnal treatment), while their respective transport parameters (both advective and diffusive), spatial grids, and numerical schemes match those

of the GSFC and LLNL models. In the AER/GSFC model, the GSFC procedure for treating tropospheric H_2O has also been adopted. The top boundary of the AER/LLNL model is at 80 km (as in the native LLNL model), while the top boundary of the AER/GSFC model is at 60 km (not 90 km as in the GSFC model). The following inert tracer experiment has been used to test whether the LLNL and GSFC transport formulations have been implemented correctly within the hybrid models, and how closely the implementation matches the native model.

3.2. Inert Tracer Comparison

[26] The Models and Measurements II experiment A-3 [*Park et al.*, 1999] has been used to test the accuracy of the transport implementation in the hybrid models. This experiment simulates the NO_y perturbation due to a fleet of 500 supersonic aircraft cruising at Mach 2.4, with most emissions occurring in the Northern Hemisphere at altitudes of 18–20 km. The source is taken from the 1995 NASA HSCT scenario [*Stolarski et al.*, 1995] with NO_x emissions of 10 grams NO_2 per kilogram of aircraft fuel burned. Background NO_y is zero. Removal in the troposphere is simulated by setting a boundary condition of zero concentration below 6 km. There is no stratospheric removal.

[27] October distributions of the A-3 tracer simulated by the AER, AER/GSFC, AER/LLNL, GSFC, and LLNL models are shown in Figure 2. Comparison of the results from the native models (Figures 2a, 2d, and 2e) shows that the GSFC model retains the most emitted material in the stratosphere (80% more than the AER model and 65% more than the LLNL model). Consequently, the GSFC model transports the most tracer to the upper stratosphere and to the Southern Hemisphere (by more than a factor of two). When these results are scaled to represent equal atmospheric burdens of injected tracer, the GSFC model obtains 18% more tracer at 45°S and 20 km than the AER model and 29% more than the LLNL model, indicating that the models differ in their global distributions of tracer. Differences between the native models and their corresponding hybrids reflect the extent to which the hybrid model transport does not reproduce the native model. Differences between the GSFC and AER/GSFC models are less than 1% throughout the stratosphere. Differences between the LLNL and AER/LLNL models are at most 3%. In the region near the tropopause where gradients are large, application of the GSFC and LLNL numerical schemes within the AER model was necessary to achieve this level of similarity in the hybrid models. Overall, the results from the A-3 calculations demonstrate that both hybrid models faithfully represent transport characteristics of their respective native models.

4. Background Atmosphere Intercomparison

[28] The hybrid models have been employed to distinguish between chemical and transport effects on intermodel differences in simulated distributions of chemical species in the background atmosphere. These distributions correspond to the Atmospheric Effects of Aviation Program (AEAP) calculations for a 2015 atmosphere with subsonic aircraft [*IPCC*, 1999; *Kawa et al.*, 1999], labeled scenario D in the work of *IPCC* [1999]. The 2015 atmosphere is assumed to contain a stratospheric Cl_y concentration of 3.0 ppbv, N_2O surface concentration of 330 ppbv, and background (nonvolcanic) levels of stratospheric aerosol. Each of the calculations represents the model's steady state (i.e., no appreciable change in the species' concentrations from one model year to the next).

[29] Because of uncertainties associated with PSC chemistry, two simulations have been performed for each model: one with and one without PSC chemistry. The results are discussed in the following format. Figure 3 shows the distributions of NO_y, H_2O, Cl_y, and O_3 from the AER model in October with the PSC parameterization. Differences among models are shown in Figures 4–13. Parts (a), (b), and (c) of Figures 4–13 show intermodel differences in calculated concentrations with a PSC parameterization for the (X-AER), (AER/X-AER), and (X-AER/X) cases, respectively, where X represents either GSFC or LLNL and AER/X is the corresponding hybrid model. Note that the sum of differences in parts (b) and (c) of Figures 4–13 equals the difference in part (a) of Figures 4–13. Differences in part (b) of Figures 4–13 are caused by differences in transport, while part (c) of Figures 4–13 represents differences in chemical formulation (in the troposphere, differences in the treatment of water vapor may also contribute). Part (d) of Figures 4–13 shows differences (X-AER/X) without the PSC parameterization. Comparison of parts (c) and (d) of Figures 4–13 isolates the impact of the PSC treatment.

[30] While the use of the 2015 background atmosphere makes observational comparisons impossible, it is useful to keep in mind that the AER model tends to calculate concentrations which are too low in the lower stratosphere for downward diffusing species (e.g., O_3, NO_y, Cl_y). Compared with the TOMS climatology, the AER model calculates too much ozone during the springtime maximum (by about 10–15%), and underpredicts ozone column in the tropics by about 5–10%.

4.1. NO_y

[31] Figure 3a shows the distribution of total odd nitrogen (NO_y) calculated by the AER model for October. A maximum value of 21 ppbv is calculated in the tropics at around 40 km, falling off to 10 ppbv at 50 km and 30 km. At higher latitudes, the maximum NO_y value (about 15 ppbv) is found near 30 km. Both the GSFC and LLNL native models (Figures 4a and 5a) calculate more NO_y than the AER model in the middle and upper stratosphere, with maximum mixing ratios of 25 ppbv. The LLNL model exhibits both positive and negative differences from the AER model in the lower stratosphere, while the GSFC model has positive differences everywhere above 20 km. Transport differences (shown in Figures 4b and 5b) cause relatively large positive and negative differences in NO_y, which often account for about half of the total differences. Since the hybrid models remove the effects of different transport, the differences shown in Figures 4c and 5c are the result of different chemistries (e.g., NO_y production from N_2O and lightning, gas phase removal by NO photolysis followed by the N + NO reaction, removal by PSC chemistry, and washout in the troposphere). Results from Figures 4d and 5d demonstrate that the effect of PSCs is limited to 50–90°S at 10–25 km altitude in October.

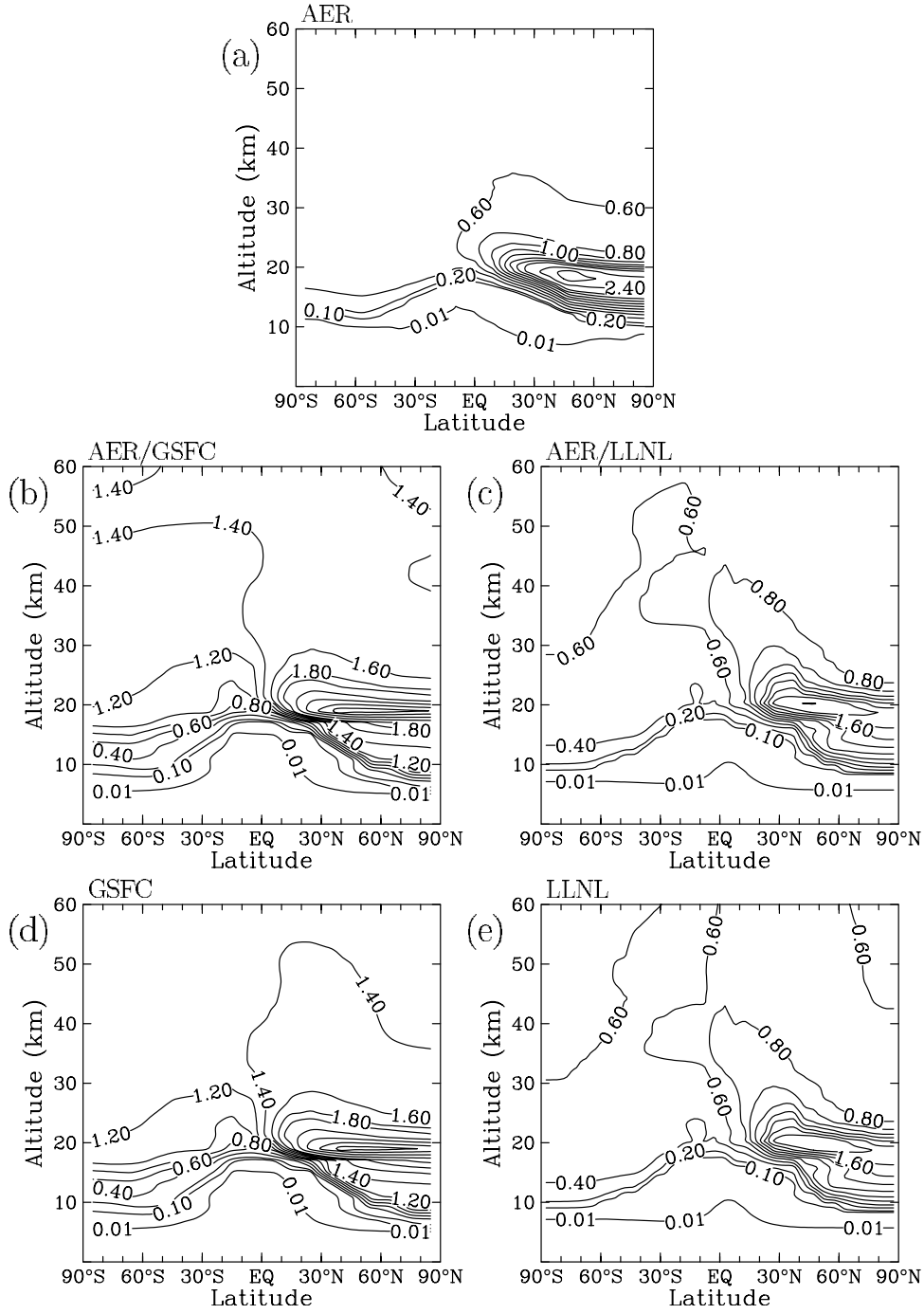

Figure 2. Calculated mixing ratio (ppbv) for October of an inert tracer with source similar to HSCT aircraft emission of NO_y and tropospheric sink. (a) AER model results. (b) AER/GSFC results. (c) AER/LLNL results. (d) GSFC results. (e) LLNL results. Contours are 0.01, 0.1, 0.2–2.0 by 0.2, and 2.4–3.6 by 0.4.

[32] Both the GSFC and LLNL chemical formulations (see Figures 4c and 5c) calculate up to 6 ppbv more NO_y in the upper stratosphere than the AER chemical formulation, which is most likely due to differences in NO photolysis (J(NO)) between the models since this reaction is the only stratospheric removal of NO_y outside the winter polar regions where PSCs cause denitrification. This was confirmed by a calculation with the LLNL model using values of J(NO) obtained from the AER model. The AER/LLNL model-calculated NO_y is similar to that calculated by the LLNL model in the low latitude middle stratosphere, indicating minimal chemical differences between the two models in this region. NO_y differences in the high latitude lower stratosphere are likely due to transport from higher altitudes. The GSFC model and AER/GSFC model exhibit differences of up to 4 ppbv of NO_y throughout the lower stratosphere, which could be due to high latitude transport from the upper stratosphere followed by horizontal mixing,

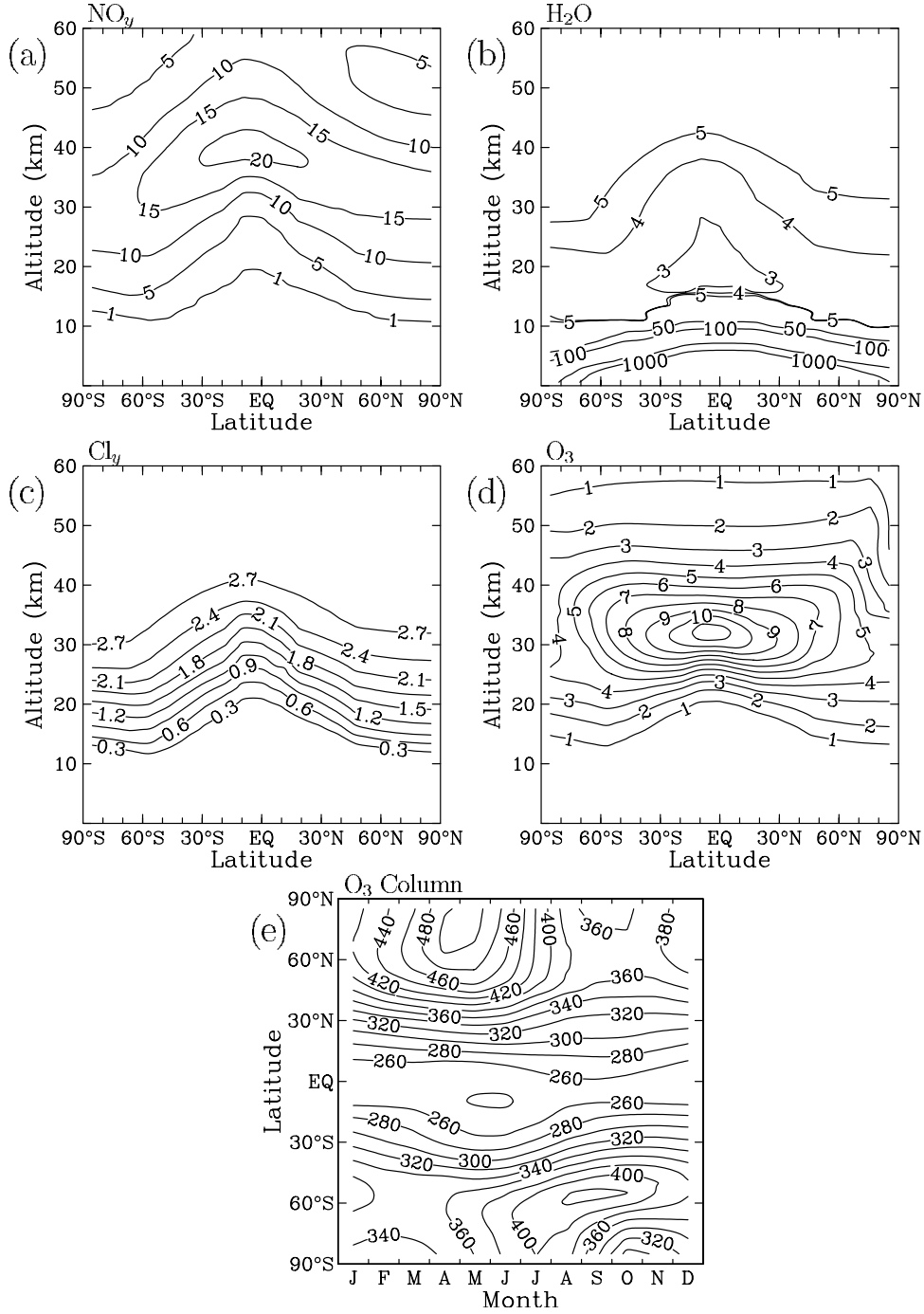

Figure 3. October mixing ratios of (a) NO_y in ppbv, (b) H_2O in ppmv, (c) Cl_y in ppbv, (d) O_3 in ppmv, and (e) total O_3 column in Dobson units as calculated by the AER model for steady state 2015 conditions.

as K_{yy} values in the GSFC transport are much larger than those in the LLNL transport.

4.2. H_2O

[33] Figure 3b shows the gas phase H_2O distribution calculated by the AER model for October. As shown in Figure 6a, the native GSFC model calculates up to 1 ppmv more H_2O in the lower and middle stratosphere than the AER model. A comparison between Figures 6b and 6c demonstrates that most of these positive differences are caused by transport. The chemical differences are negative in the whole stratosphere, between 0.5 and 1.0 ppmv between 40 and 60 km, and less than 0.5 ppmv below 40 km. In the upper stratosphere, chemical and transport differences are of opposite sign and in places result in no net difference between the AER and GSFC model-calculated H_2O. It should be noted that the implementation of the GSFC tropospheric boundary condition for H_2O in the AER/GSFC model has greatly reduced the differences between the GSFC and AER/GSFC models in the troposphere (compare Figure 6c with Figure 6a). While it is tempting to speculate that the negative tropospheric differ-

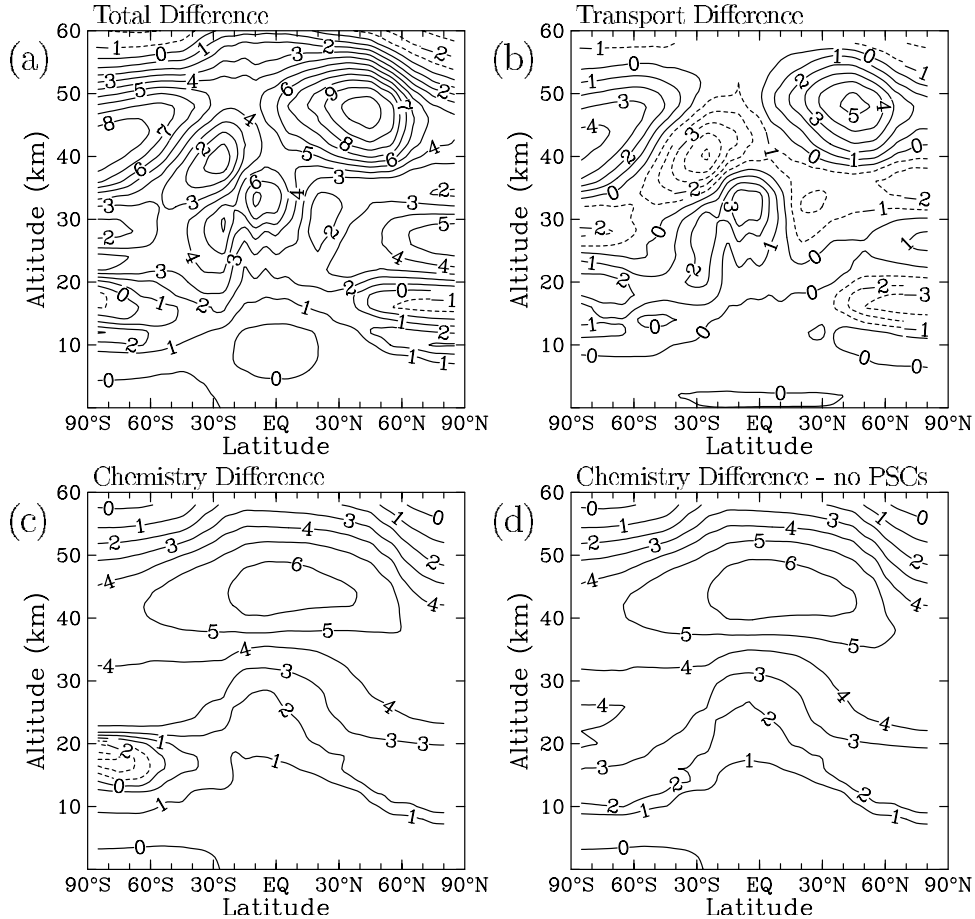

Figure 4. October NO_y mixing ratio differences (ppbv) between the GSFC and AER models in a 2015 background atmosphere with subsonic aircraft. (a) The difference between the GSFC and AER models with PSC chemistry included. (b) The difference between the AER/GSFC and AER models. (c) The difference between the GSFC and AER/GSFC models. (d) The difference between the GSFC and AER/GSFC models without PSC chemistry.

ences in Figure 6c give raise to the negative differences in the stratosphere, it should be noted that the stratospheric chemical differences in Figure 6c are similar to those for the LLNL model (Figure 7c), despite positive tropospheric differences between the LLNL and the AER/LLNL models.

[34] The native LLNL model also calculates more H_2O than the AER model in the lower stratosphere and much of the middle and upper stratosphere (Figure 7a). As in the case of the GSFC versus AER comparison, both transport and chemistry play roles in the model differences, often with offsetting effects. Both hybrid models calculate more H_2O in the middle and upper stratosphere than the comparable native model (GSFC or LLNL), an indication that the photolysis of H_2O is too weak in the AER model chemistry (because wavelengths below 177 nm are not considered). Figures 6d and 7d show that differences in PSC treatments have a small effect in October in both cases.

4.3. Cl_y

[35] The distribution of total inorganic chlorine (Cl_y) calculated by the AER model for October is shown in Figure 3c. The differences among the native models (Figures 8a and 9a) in the upper stratosphere are less than 5%, thus demonstrating that each model achieves an inorganic chlorine content in the upper stratosphere roughly equal to the input of organic chlorine in the troposphere. The differences are much larger in the lower stratosphere, approaching a factor of 2. Transport is responsible for the bulk of the differences (see Figures 8b and 9b). Figures 8c and 9c exhibit small differences due to chemistry, which could be caused by differences in family groupings or small differences in photolysis rates. PSC treatments have a negligible effect on Cl_y.

4.4. Ozone

[36] Figure 3d shows the O_3 distribution calculated by the AER model for October. In the equatorial middle stratosphere and the midlatitude lower to middle stratosphere, the native GSFC (Figure 10a) and LLNL (Figure 11a) models show less O_3 (by as much as 15% or 1.5 ppmv) than the AER model. About 2/3 of this difference in the tropics is due to transport and the remainder due to chemistry (see Figures 10b and 10c and 11b and 11c). In the upper stratosphere, both the GSFC and the LLNL models calculate more ozone in the upper stratosphere than their respective hybrid models (Figures 10c and 11c). This upper stratospheric difference remains even when both the H_2O and NO_y fields from the GSFC or LLNL models are

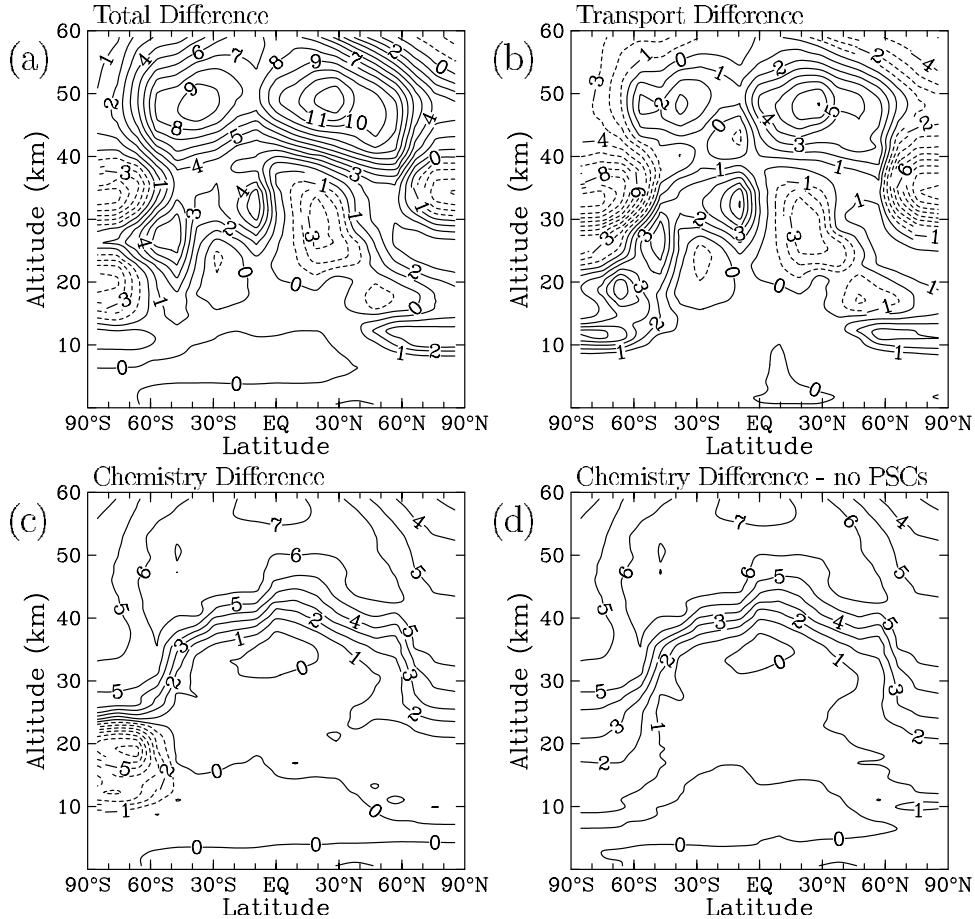

Figure 5. October NO_y mixing ratio differences (ppbv) between the LLNL and AER models in a 2015 background atmosphere with subsonic aircraft. (a) The difference between the LLNL and AER models with PSC chemistry included. (b) The difference between the AER/LLNL and AER models. (c) The difference between the LLNL and AER/LLNL models. (d) The difference between the LLNL and AER/LLNL models without PSC chemistry.

imposed in the AER/GSFC or AER/LLNL models. The AER chemical scheme is found to calculate 5–10% greater ozone photolysis than the other models in the upper stratosphere, resulting in a larger O/O_3 ratio and more efficient ozone removal. The different chemical schemes may also have differences in their partitioning of NO_y, Cl_y, Br_y, or HO_x species which would affect ozone loss. In the 20–40 km altitude range, the GSFC and LLNL models calculate less ozone than the hybrids, mainly as a result of producing more NO_y there. In the southern high latitudes in October, chemistry accounts for most of the difference between the AER and GSFC models, specifically the PSC treatment (compare Figures 10c and 10d). The comparison between the AER and LLNL models in the southern high latitudes shows that effects of transport and chemistry largely offset each other in October. The inclusion of PSCs leads to positive differences between the LLNL and AER/LLNL models. With identical transport and no PSCs, the AER/GSFC model reproduces the native GSFC model to within 0.5 ppmv, and the AER/LLNL model reproduces the native LLNL model within 0.75 ppmv.

[37] The results from comparisons of calculated ozone column are given in Figures 12 and 13. Both the GSFC and the LLNL models calculate more O_3 in the tropics and less O_3 at high latitudes than the AER model (generally resulting in better agreement with TOMS observations). The LLNL model also calculates more O_3 in the midlatitudes than the AER model. Both chemistry and transport play significant roles in the differences, often with offsetting effects. In the Southern Hemisphere high latitudes, the GSFC model calculates up to 100 DU less total ozone than the AER model. Transport differences between the AER and GSFC models lead to more ozone in austral summer and less in austral winter. In the absence of PSCs (see Figure 12d), chemical differences account for a difference of less than 20 DU, except at high southern latitudes in spring, when the GSFC model calculates 45 DU more than the AER/GSFC model. This larger calculated ozone is caused by the neglect of zonal variability in temperature when treating chemistry on sulfate aerosols. The inclusion of PSCs greatly reduces the ozone column in the GSFC model relative to the AER model. In the AER versus LLNL model comparisons, transport accounts for most of the larger ozone column amounts at southern midlatitudes in the LLNL model. The LLNL diffusion coefficients are generally very small, resulting in little mixing between the high latitudes, where ozone is destroyed, and the lower latitudes, where ozone is produced. Chemical differences without PSCs between

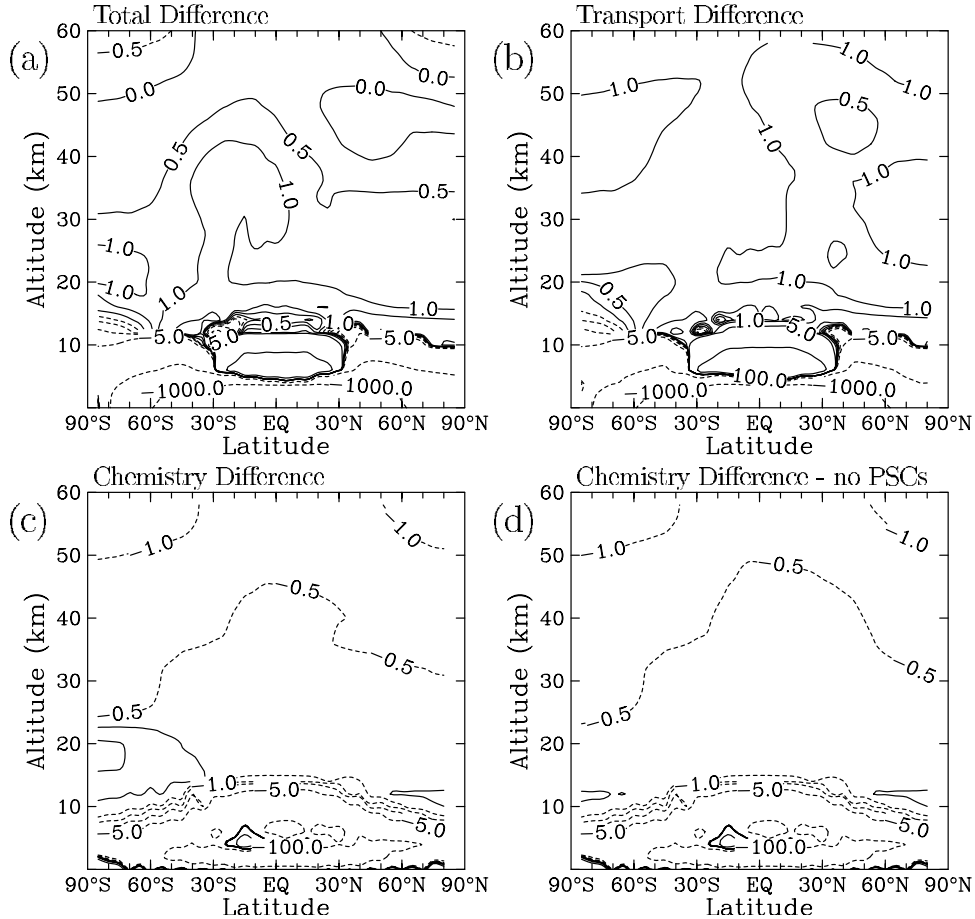

Figure 6. October H_2O mixing ratio differences (ppmv) between the GSFC and AER models in a 2015 background atmosphere with subsonic aircraft. (a) The difference between the GSFC and AER models with PSC chemistry included. (b) The difference between the AER/GSFC and AER models. (c) The difference between the GSFC and AER/GSFC models. (d) The difference between the GSFC and AER/GSFC models without PSC chemistry.

LLNL and AER are mostly 10 DU or less (Figure 13d). When PSCs are included, the LLNL model chemistry depletes ozone less efficiently than the AER chemical mechanism, thus the LLNL model has more ozone in the springtime southern high latitudes than the AER/LLNL model (Figure 13c).

5. HSCT Perturbations

[38] Over the past few decades there has been much interest in a potential fleet of commercial supersonic aircraft and its atmospheric impact. There have been numerous modeling studies to investigate the impact of High Speed Civil Transport (HSCT) aircraft in the lower stratosphere and upper troposphere [*IPCC*, 1999; *Kawa et al.*, 1999, and references therein]. These studies consist of various scenarios used to explore the effects of parametric modifications in the HSCT aircraft fleet size, cruise altitude, emission parameters, and the background atmosphere. The model response can be generally explained in terms of the amount of engine emissions retained in the stratosphere (a transport issue), and the response of ozone to these perturbations (where both transport and chemistry play a role). It is the latter complication that makes it difficult to separate the two effects and intercompare model results in a clear-cut fashion.

[39] In order to diagnose the cause of intermodel differences documented in the *IPCC* [1999] report (to which the AER, GSFC and LLNL groups contributed their results), we have performed additional calculations with the AER/GSFC and the AER/LLNL hybrid models described in this paper. To be specific, we have focused on scenario S1c from *IPCC* [1999], which represents a fleet of 500 HSCT aircraft operating in 2015, with a NO_x emission index of 5 grams of NO_2 per kilogram of fuel burned and H_2O emission index of 1230 grams per kilogram of fuel. The aircraft have a cruise altitude of 18–20 km and fly predominantly in the Northern Hemisphere, but with some emissions deposited in the tropics and between 20°S and 40°S. The resulting chemical perturbations are computed by comparing this scenario with scenario D discussed in section 4.

[40] Scenario S1c was calculated by nine modeling groups for the *IPCC* [1999] assessment report. Annual average ozone column perturbations ranged from 0.0% to −0.4% for the Northern Hemisphere and from 0.0% to −0.8% for the Southern Hemisphere [*IPCC*, 1999]. This wide range in ozone response was difficult to interpret at that time, since transport and chemical effects could not be

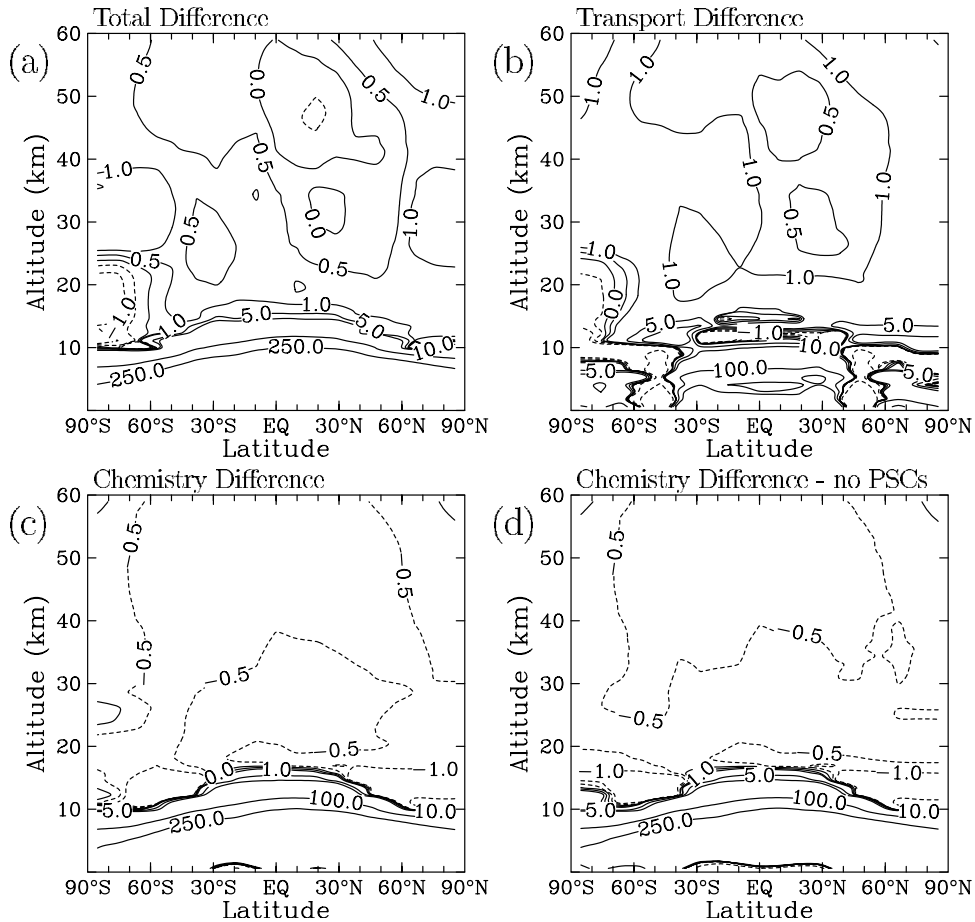

Figure 7. October H_2O mixing ratio differences (ppmv) between the LLNL and AER models in a 2015 background atmosphere with subsonic aircraft. (a) The difference between the LLNL and AER models with PSC chemistry included. (b) The difference between the AER/LLNL and AER models. (c) The difference between the LLNL and AER/LLNL models. (d) The difference between the LLNL and AER/LLNL models without PSC chemistry.

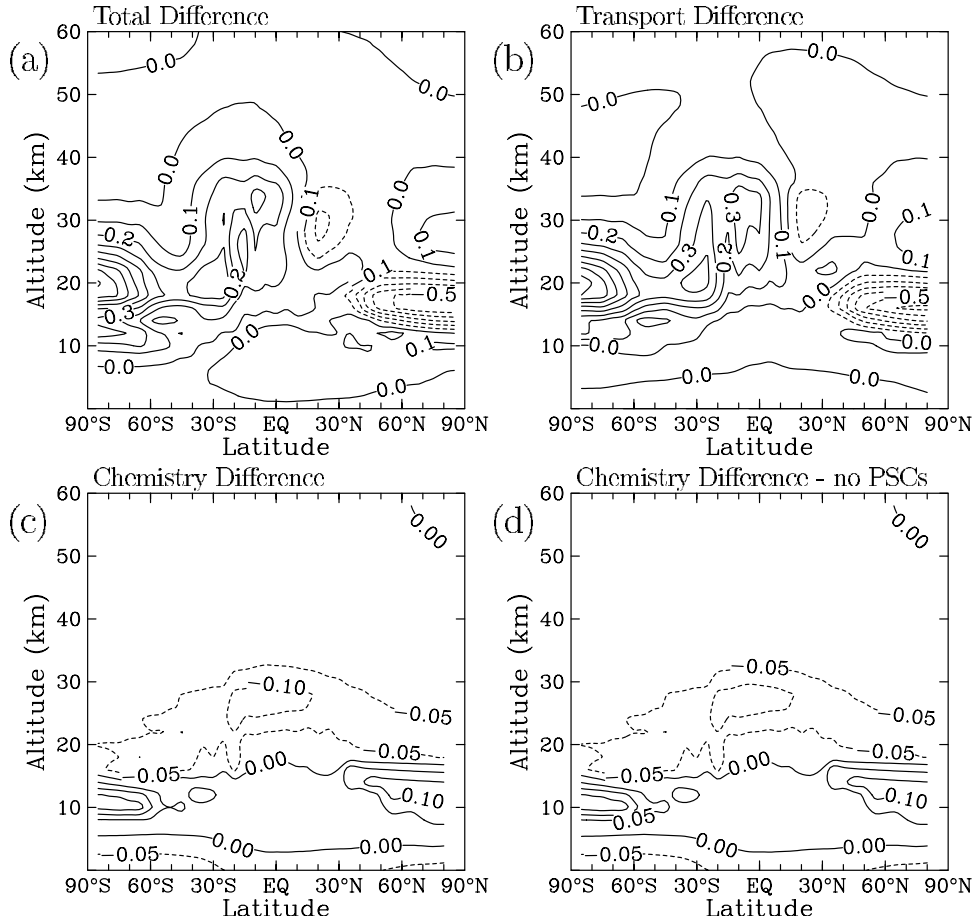

Figure 8. October Cl_y mixing ratio differences (ppbv) between the GSFC and AER models in a 2015 background atmosphere with subsonic aircraft. (a) The difference between the GSFC and AER models with PSC chemistry included. (b) The difference between the AER/GSFC and AER models. (c) The difference between the GSFC and AER/GSFC models. (d) The difference between the GSFC and AER/GSFC models without PSC chemistry.

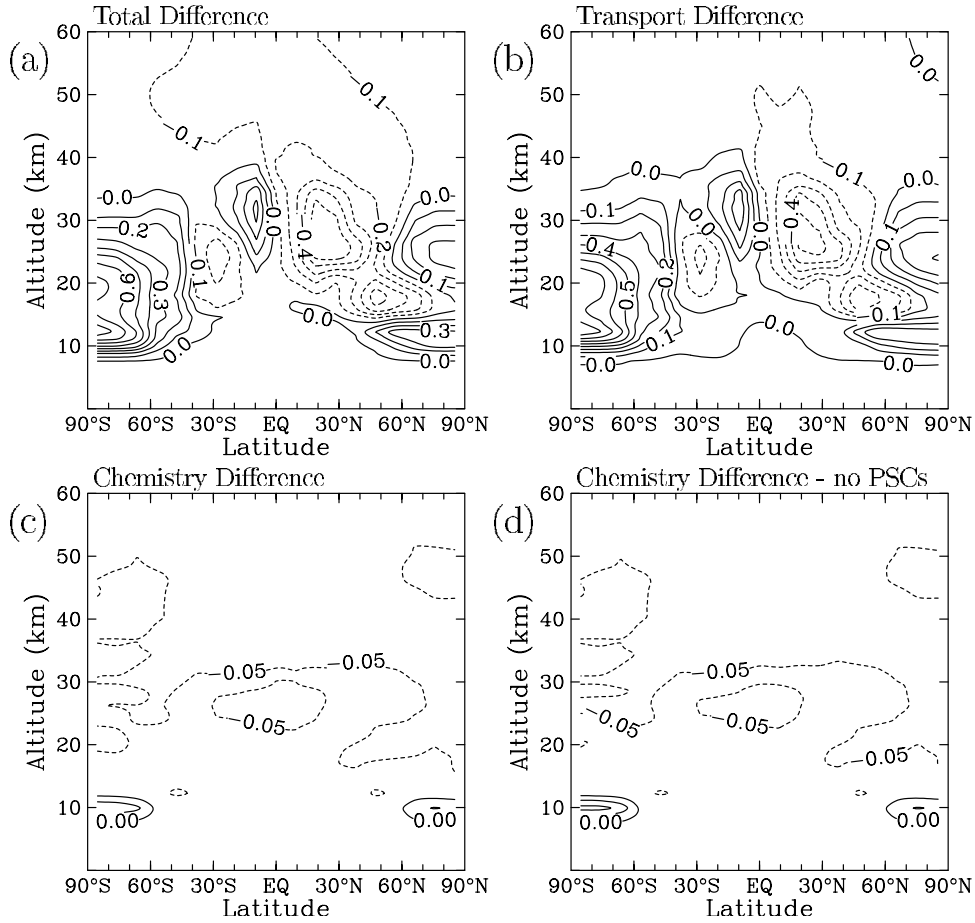

Figure 9. October Cl_y mixing ratio differences (ppbv) between the LLNL and AER models in a 2015 background atmosphere with subsonic aircraft. (a) The difference between the LLNL and AER models with PSC chemistry included. (b) The difference between the AER/LLNL and AER models. (c) The difference between the LLNL and AER/LLNL models. (d) The difference between the LLNL and AER/LLNL models without PSC chemistry.

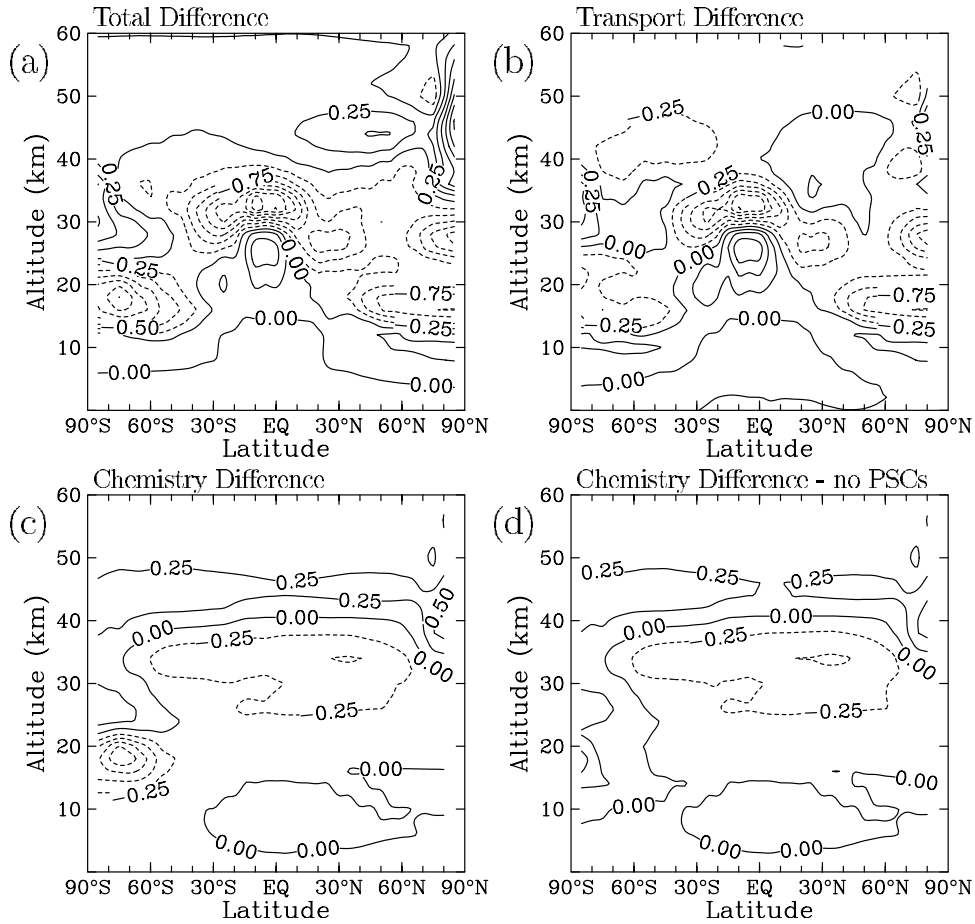

Figure 10. October O_3 mixing ratio differences (ppmv) between the GSFC and AER models in a 2015 background atmosphere with subsonic aircraft. (a) The difference between the GSFC and AER models with PSC chemistry included. (b) The difference between the AER/GSFC and AER models. (c) The difference between the GSFC and AER/GSFC models. (d) The difference between the GSFC and AER/GSFC models without PSC chemistry.

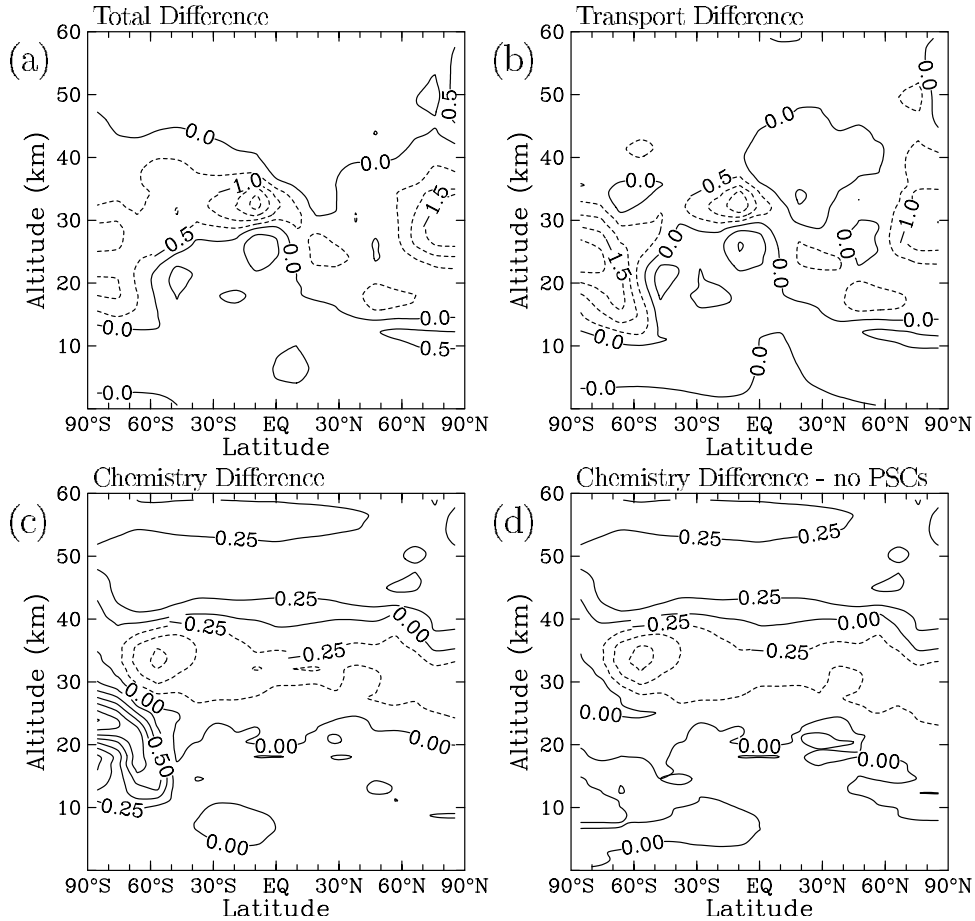

Figure 11. October O_3 mixing ratio differences (ppmv) between the LLNL and AER models in a 2015 background atmosphere with subsonic aircraft. (a) The difference between the LLNL and AER models with PSC chemistry included. (b) The difference between the AER/LLNL and AER models. (c) The difference between the LLNL and AER/LLNL models. (d) The difference between the LLNL and AER/LLNL models without PSC chemistry.

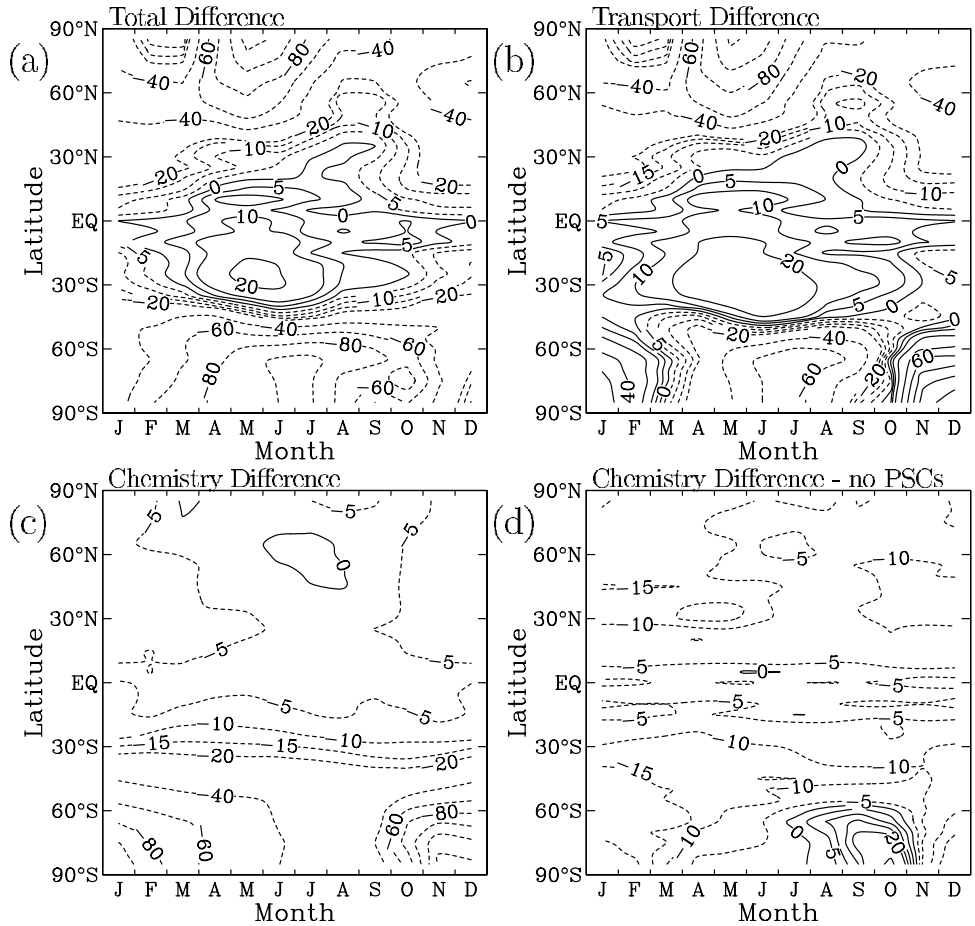

Figure 12. O_3 column differences (Dobson units) between the GSFC and AER models in a 2015 background atmosphere with subsonic aircraft. (a) The difference between the GSFC and AER models with PSC chemistry included. (b) The difference between the AER/GSFC and AER models. (c) The difference between the GSFC and AER/GSFC models. (d) The difference between the GSFC and AER/GSFC models without PSC chemistry. Contours are −140 to 140 by 20 and −15 to 10 by 5.

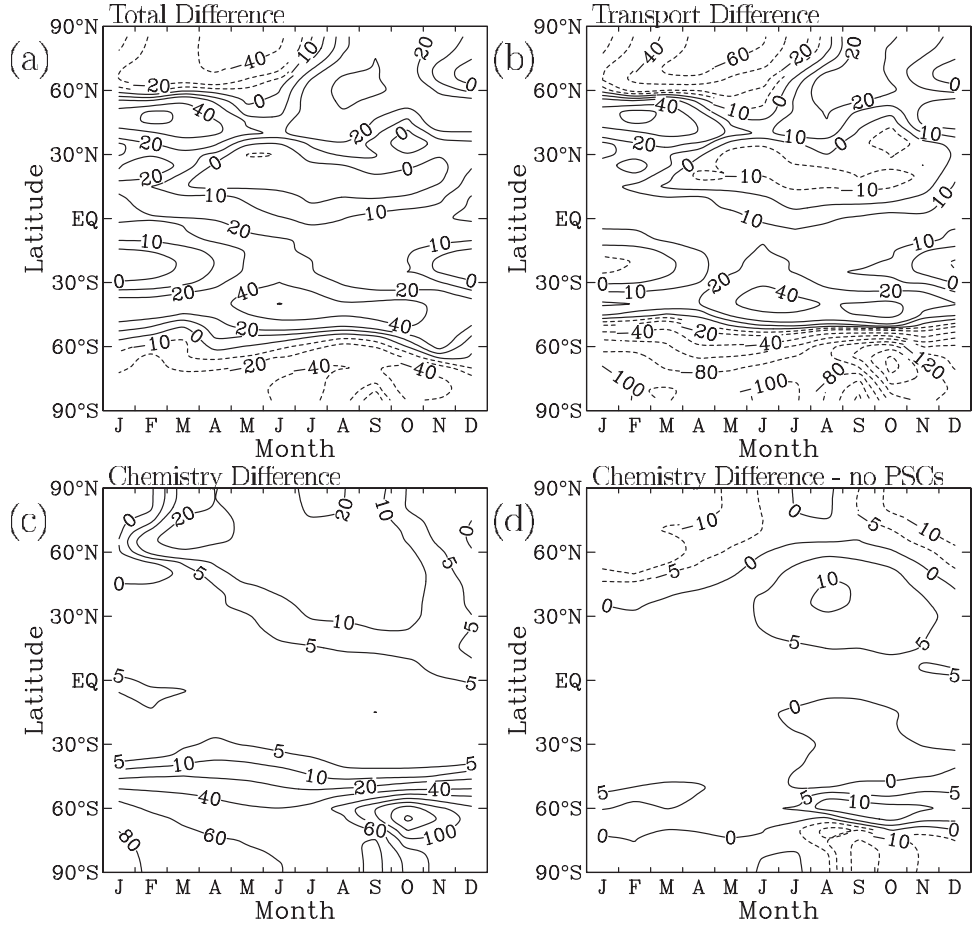

Figure 13. O_3 column differences (Dobson units) between the LLNL and AER models in a 2015 background atmosphere with subsonic aircraft. (a) The difference between the LLNL and AER models with PSC chemistry included. (b) The difference between the AER/LLNL and AER models. (c) The difference between the LLNL and AER/LLNL models. (d) The difference between the LLNL and AER/LLNL models without PSC chemistry. Contours are −160 to 140 by 20, plus −10 and 10 DU contours in all panels and −5 and 5 DU contours in Figures 13c and 13d.

easily separated. By examining perturbations of O_3 column, local O_3, H_2O, and NO_y using the AER/GSFC and the AER/LLNL hybrid models, we can gain insights into how the different model chemical formulations affect the HSCT ozone perturbations. To simplify interpretation, we will discuss calculations without PSC chemistry first, followed by a discussion of the O_3 perturbation results with PSC chemistry included, which has quite a large impact on these calculations.

[41] Perturbations to H_2O and NO_y for October without PSC chemistry are shown in Figures 14 and 15, respectively. The H_2O results are similar to those for the inert tracer shown in Figure 2 when scaled for emissions (factor of 0.31). The NO_y results scale by 0.5 from results shown in Figure 2 except that NO_y has chemical loss in the upper stratosphere. As in experiment A-3, more emissions are transported to the Southern Hemisphere in the GSFC model than the AER or LLNL models. The HSCT NO_y and H_2O perturbation differences between the native GSFC and LLNL models and their respective hybrids are small, despite the fairly large differences between the NO_y and H_2O background concentrations, indicating that transport plays the major role in this case.

[42] Perturbations in O_3 for October due to HSCT emissions without PSC chemistry are shown in Figure 16. The GSFC and AER/GSFC models show twice as much O_3 depletion in the upper stratosphere as the LLNL and AER/LLNL models and almost three times as much as the AER model, which is mainly a response to the H_2O perturbation in this region. Models with similar transport show similar ozone depletion in the upper stratosphere, indicating that the ozone perturbation is responding to the perturbations in NO_y and H_2O but is not very sensitive to background concentrations of these gases in the upper stratosphere. The GSFC and AER/GSFC hybrid models show large differences in the lower stratosphere. These differences could be due to the different background levels of NO_y, Cl_y, Br_y, and H_2O in this region or to different chemical treatment of O_3. To separate these effects, we have repeated some calculations with the AER/GSFC hybrid model imposing the NO_y, H_2O, Cl_y, and Br_y from the GSFC model for both background and HSCT conditions. This calculation does not show an ozone increase outside the tropics in the lower stratosphere, in contrast to Figure 16b. The background NO_y concentration is found to be the major cause of the change. The Southern Hemi-

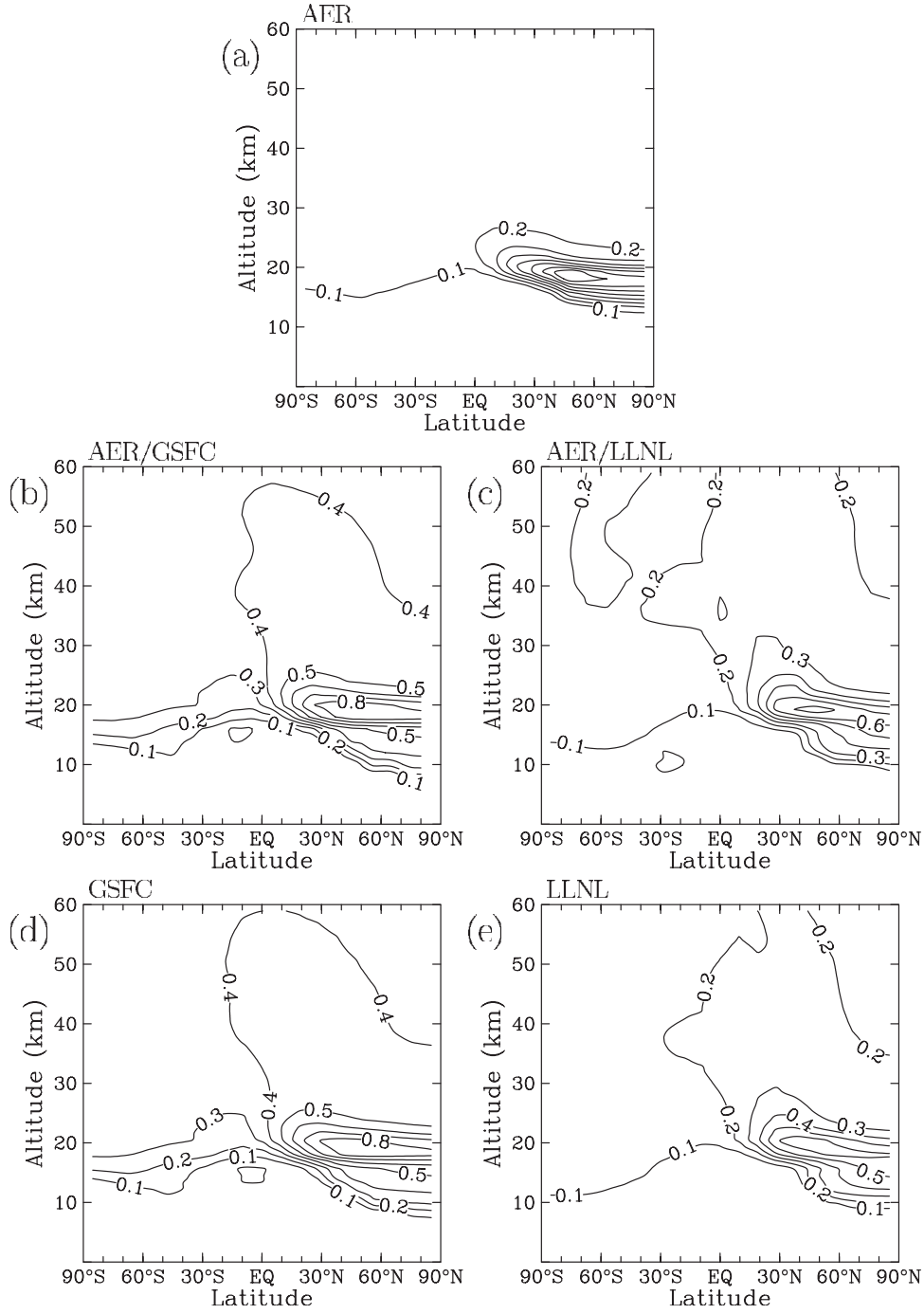

Figure 14. Calculated perturbation in H_2O (ppmv) for October due to emission from HSCT aircraft in 2015 relative to an atmosphere with only subsonic aircraft. (a) AER model results. (b) AER/GSFC results. (c) AER/LLNL results. (d) GSFC results. (e) LLNL results. All calculations are without PSC chemistry.

sphere lower stratosphere shows ozone decreases similar to the native GSFC results shown in Figure 16d, but the Northern Hemisphere lower stratosphere is very different. These differences must be due to difference in ozone chemistry and not to differences in the background amounts of NO_y, Cl_y, Br_y, or H_2O. A similar experiment with the AER/LLNL model shows little change above 20 km, but differences due to background levels of trace gases below 20 km. The AER/LLNL hybrid model, even with NO_y, Cl_y, Br_y, and H_2O fields from the LLNL model, does not reproduce the strong October southern polar ozone decrease at 8–18 km seen in Figure 16e.

[43] Figure 17 shows perturbations in O_3 column for simulations without PSC chemistry. Of the native models, the LLNL model shows the greatest O_3 depletion at both poles. The GSFC model shows the least depletion at the north pole, but the most at 30°N. The GSFC and AER/GSFC models both show a maxima of O_3 depletion

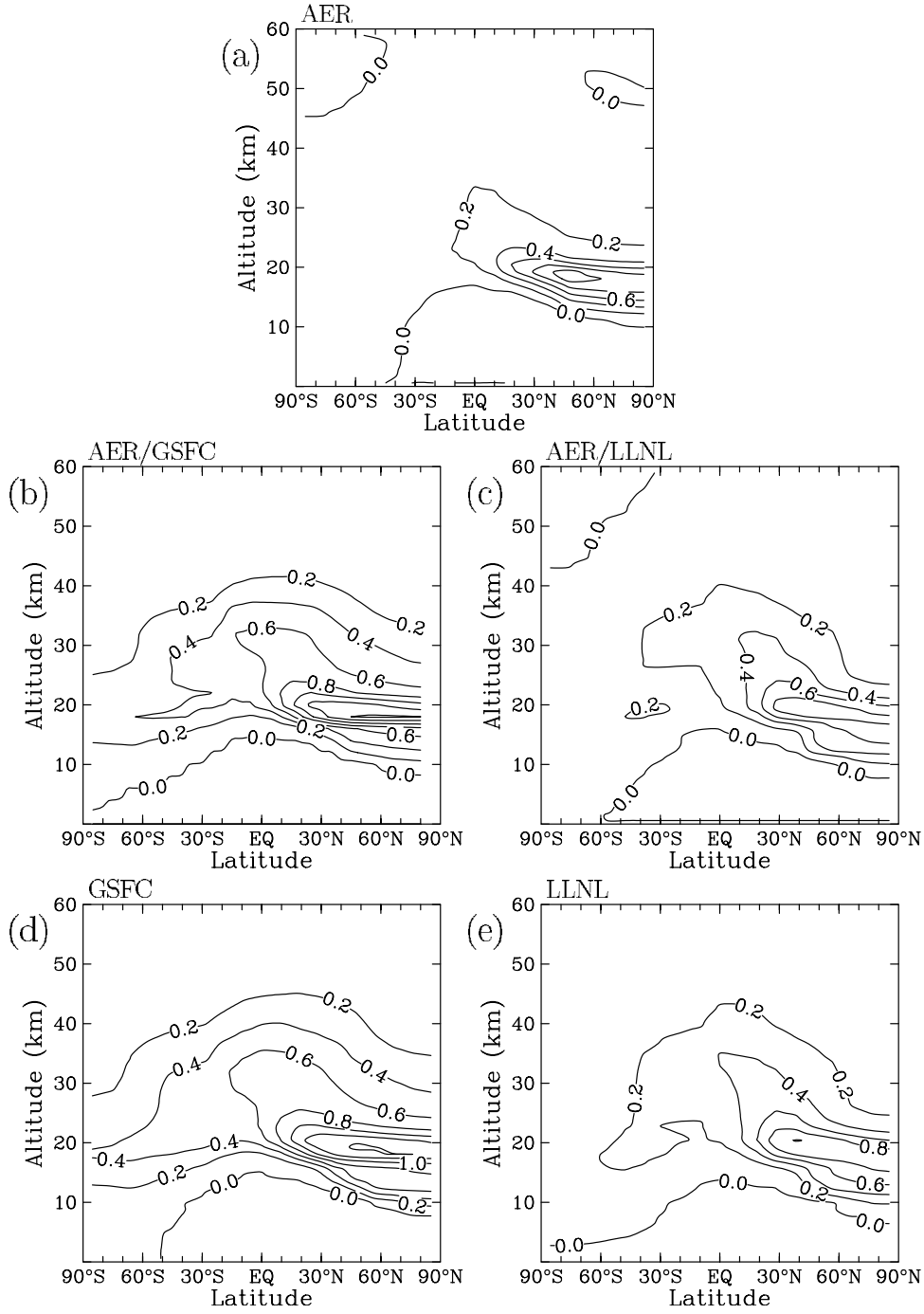

Figure 15. Calculated perturbation in NO_y (ppbv) for October due to emission from HSCT aircraft in 2015 relative to an atmosphere with only subsonic aircraft. (a) AER model results. (b) AER/GSFC results. (c) AER/LLNL results. (d) GSFC results. (e) LLNL results. All calculations are without PSC chemistry.

at 30°N, indicating that this is a feature of the GSFC transport (a result of the O_3 enhancement from 40–90°N at 8–12 km altitude seen in Figures 16b and 16d). However, the AER/GSFC model shows a local maximum of O_3 depletion at the north pole in springtime, whereas the GSFC model does not. The AER, LLNL, and both hybrid models show only 0.1% O_3 depletion in the southern tropics, while the GSFC model shows 0.3% O_3 depletion here. A calculation with the AER/GSFC hybrid model using imposed NO_y and H_2O from the GSFC model gives 0.3% ozone depletion in the southern tropics, indicating that background NO_y levels are controlling the sensitivity of ozone to HSCT emissions here. In that case, Southern Hemisphere ozone depletion is increased to 0.4 to 0.6% and Northern Hemisphere ozone depletion to 0.8 to 1.0%, with the models becoming more divergent in the Northern Hemisphere. The LLNL and AER/LLNL models give fairly similar ozone perturbations between 45°S and 60°N.

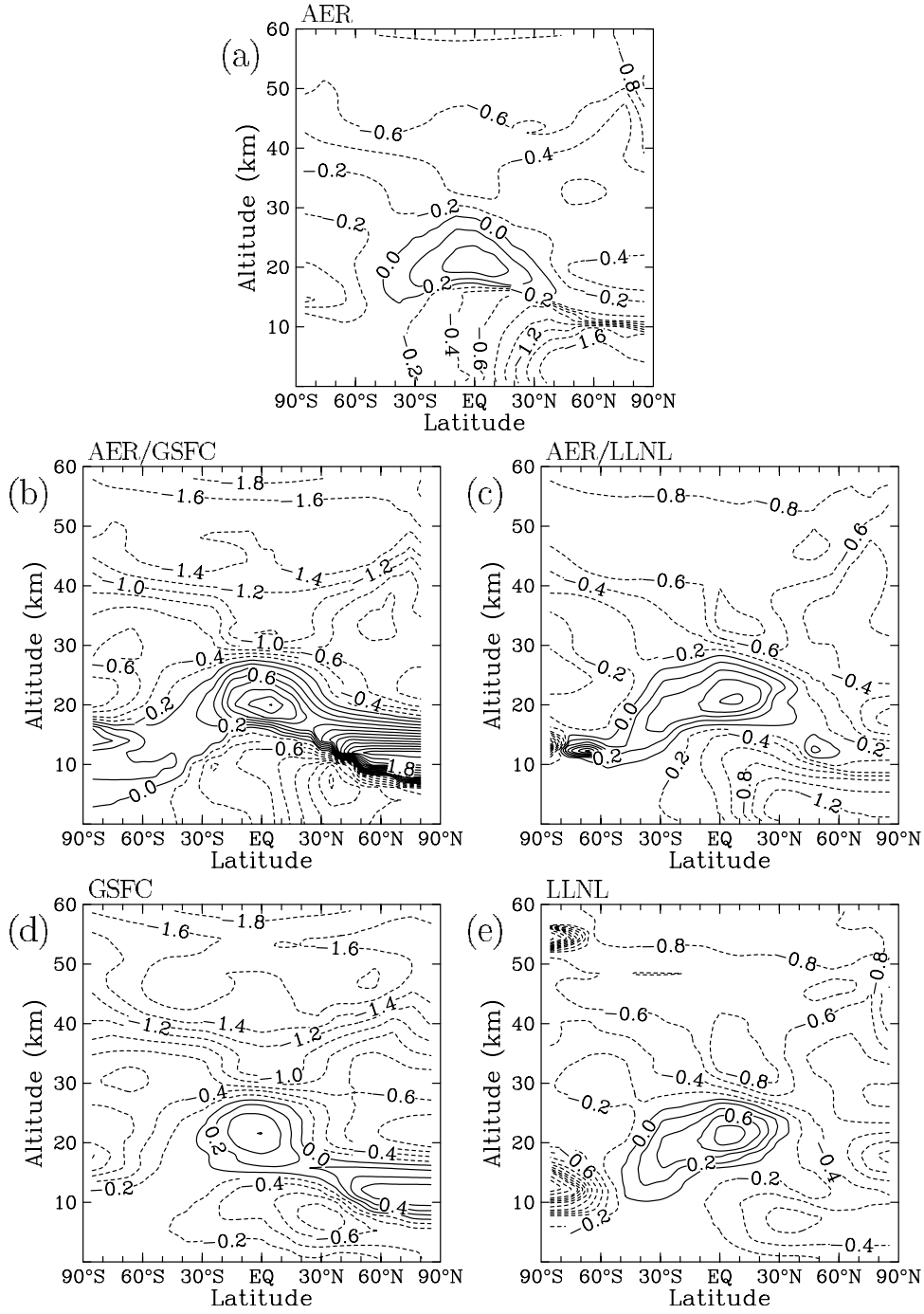

Figure 16. Calculated perturbation in O_3 (%) for October due to emission from HSCT aircraft in 2015 relative to an atmosphere with only subsonic aircraft. (a) AER model results. (b) AER/GSFC results. (c) AER/LLNL results. (d) GSFC results. (e) LLNL results. All calculations are without PSC chemistry.

[44] With PSC chemistry, all models show denitrification and dehydration at the south pole in austral spring. The GSFC model, but not the AER or LLNL models, also showsdenitrification near the north pole in springtime. O_3 perturbations for October with PSC chemistry are shown in Figure 18, and perturbations in O_3 column are shown in Figure 19. All models show enhanced O_3 depletion due to HSCT emissions in both hemispheres with PSC chemistry included, except for the LLNL model in the Northern Hemisphere. This is because HSCT emissions of H_2O and NO_y lead to enhancements in PSC surface area which activate additional chlorine and cause ozone depletion. PSC chemistry has a very large impact on calculated ozone perturbations due to HSCT at high latitudes and increases the model differences. The hybrid models show much more O_3 depletion at high northern latitudes than the GSFC and LLNL models. In fact, the larger than 1% depletions in the northern high latitudes reported by the AER model in *IPCC* [1999] are present in both hybrid models as well, indicating that this is a feature of the AER chemistry related to PSC

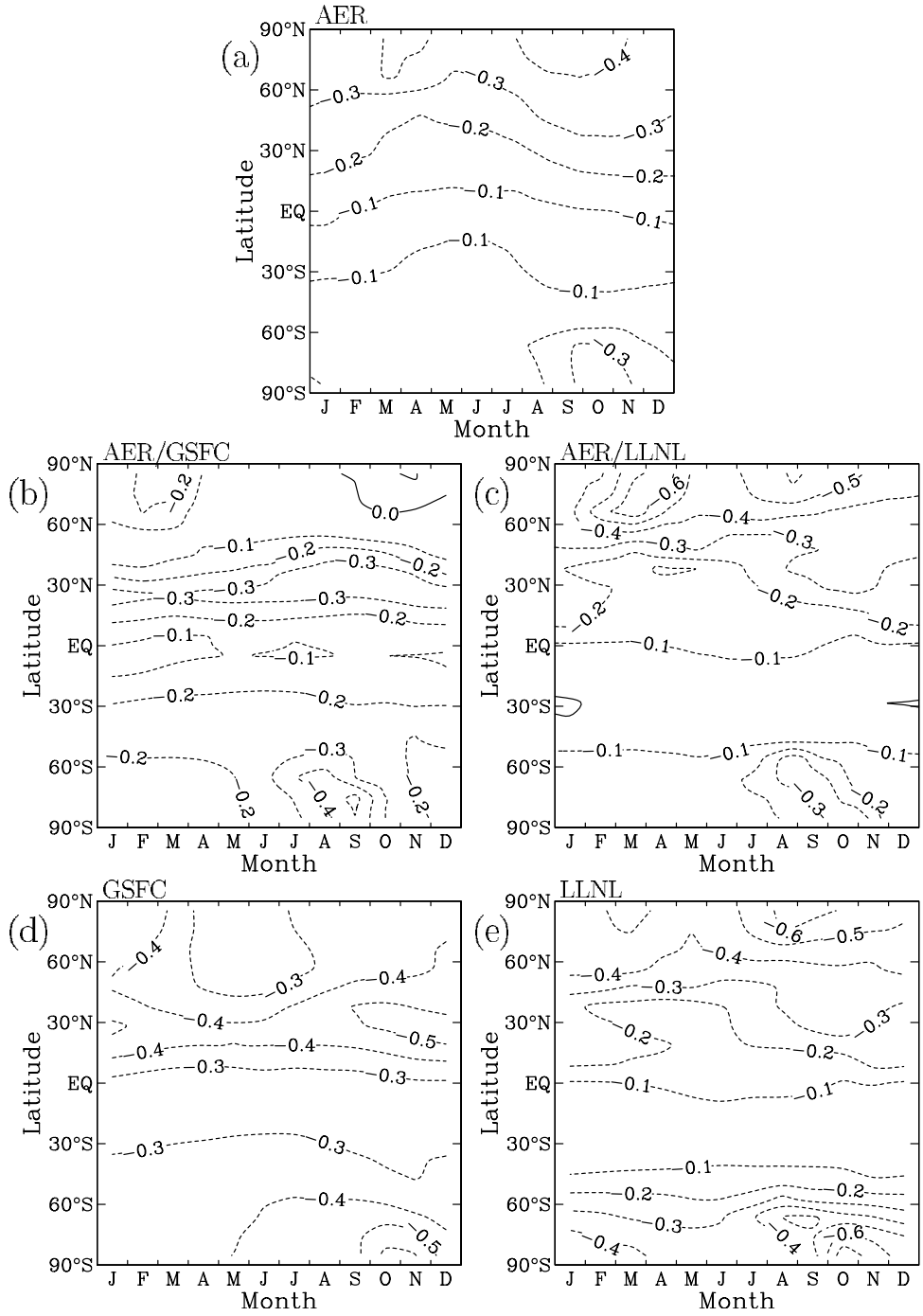

Figure 17. Calculated perturbation in total O_3 column (%) due to emission from HSCT aircraft in 2015 relative to an atmosphere with only subsonic aircraft. (a) shows AER model results. (b) AER/GSFC results. (c) AER/LLNL results. (d) GSFC results. (e) LLNL results. All calculations are without PSC chemistry.

treatment. On the other hand, the relatively modest depletions in the southern high latitudes (and their small sensitivity to the inclusion of PSCs) seen in the native AER model are a product of AER transport, as both hybrid models show very large depletions in that region. The AER model transort has little if any isolation of the southern polar vortex, and thus small sensitivity to PSC processing. Though the AER/LLNL model does not differ substantially from the AER model in the magnitude of its perturbations to H_2O and NO_y due to the aircraft emissions in the Southern Hemisphere, its transport is much less diffusive and therefore ozone responds more strongly to those perturbations.

6. Summary and Conclusions

[45] Past comparisons of model-calculated ozone perturbations are incomplete because reasons for intermodel differences, especially the relative contributions of transport

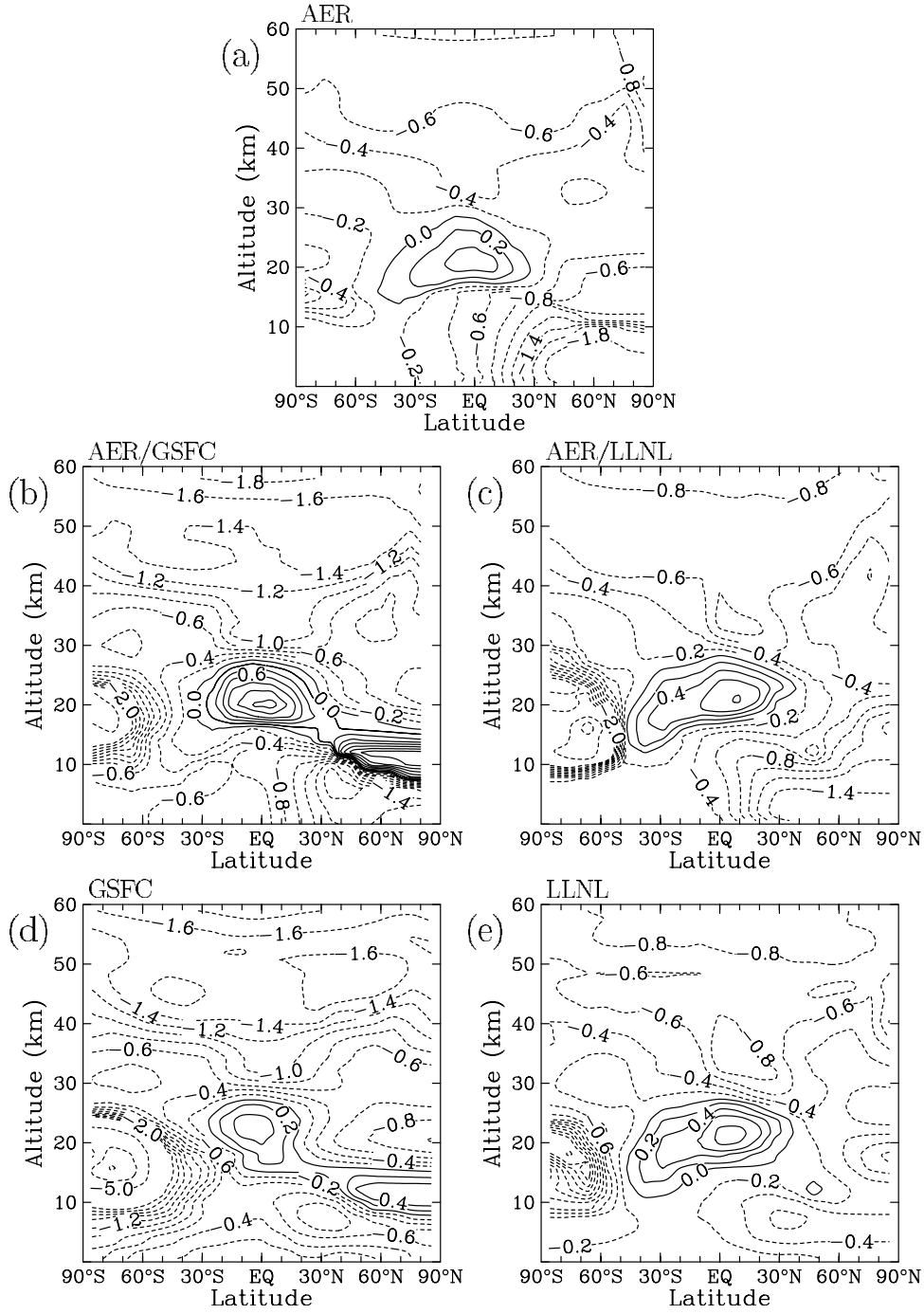

Figure 18. Calculated perturbation in O_3 (%) for October due to emission from HSCT aircraft in 2015 relative to an atmosphere with only subsonic aircraft. (a) AER model results. (b) AER/GSFC results. (c) AER/LLNL results. (d) GSFC results. (e) LLNL results. All calculations are with PSC chemistry. Contours are −2 to 1.6 by 0.2, and in addition, for Figure 18b a −3 contour, for Figure 18c −4 and −6 contours, for Figure 18d −5, −10, and −15 contours, and for Figure 18e a −2.5 contour.

and chemistry, have not been diagnosed. We have approached this problem by constructing hybrid models that combine the transport fields of the GSFC and LLNL models with the chemical formulation of the AER model. The purely chemical contribution to intermodel differences is obtained as the difference between the native (GSFC or LLNL) and the hybrid (AER/GSFC and AER/LLNL) models. The hybrid models have been validated by performing an inert tracer experiment and then applied to diagnose the chemical contribution to intermodel differences in the background atmosphere and HSCT perturbation simulations. Differences in ozone perturbations due to ozone chemistry have been separated from those due to background concentrations of NO_y, H_2O, Cl_y, and Br_y.

[46] By comparing the calculated 2015 background atmospheres from the LLNL and GSFC native models with

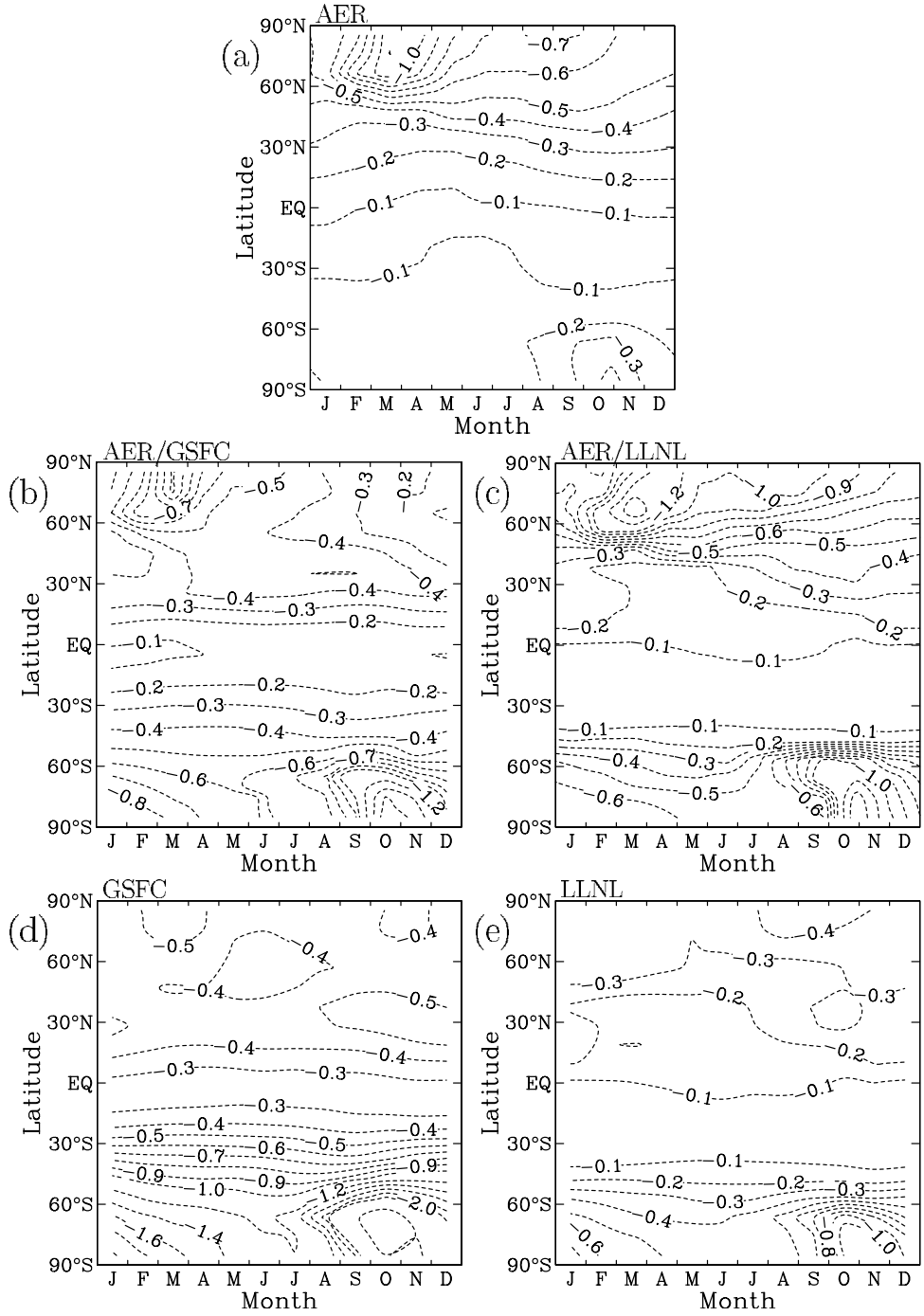

Figure 19. Calculated perturbation in total O_3 column (%) due to emission from HSCT aircraft in 2015 relative to an atmosphere with only subsonic aircraft. (a) AER model results. (b) AER/GSFC results. (c) AER/LLNL results. (d) GSFC results. (e) LLNL results. All calculations are with PSC chemistry. Contours are −2 to −1.2 by 0.2, −1.0 to −.1 by 0.1, and for Figure 19d a −3 contour.

the two hybrids, we have identified model differences due to chemistry which reflect either real uncertainties in the models due to different, but equally valid, methods of treating atmospheric processes or places where model improvements should produce agreement. The removal of NO_y in the upper stratosphere by photolysis of NO and the photolysis of H_2O have been identified as areas of the models which should be improved. Treatment of PSCs accounts for a large amount of model variability in the polar regions, but improvement here awaits further research and development of new parameterizations. Other identified differences include how a 2-D model treats deviations from the zonal mean temperature when calculating heterogeneous chemical rates on sulfate aerosol. The chemical differences between ozone calculations in the models have not been fully resolved but likely involve differences in

partitioning of NO_y, Cl_y, Br_y, and HO_x species and in ozone photolysis.

[47] In the HSCT perturbation calculations, most of the differences in the H_2O and NO_y perturbations are due to transport. Calculated ozone perturbation differences in the upper stratosphere can be attributed to differences in transport of H_2O. Differences in the lower stratosphere are more difficult to interpret, being partly due to differences in background amounts of NO_y, Cl_y, Br_y, or H_2O, partly to partitioning of the radical species which contribute to ozone loss, and partly to transport of ozone. We find that the larger than 1% O_3 column depletions in the HSCT S1c scenario for the AER model with PSCs quoted in the *IPCC* [1999] report reflect AER's chemistry under PSC conditions, as they are present in both hybrid models as well. In contrast, the relatively small depletions in the Southern Hemisphere reflect AER transport, specifically the large and spatially uniform values of horizontal diffusion, as Southern Hemisphere ozone depletion in the hybrid models is greatly enhanced over that seen in the AER model.

[48] This study has allowed us to quantitatively diagnose transport and chemical differences between three of the models participating in the IPCC assessment [*IPCC*, 1999], and this has led to improvements in the models. For example, because of the NO_y differences identified in this study, the LLNL model has modified J(NO) by creating a new lookup table for this parameter derived from AER results (i.e., the *Prather* [1993] photolysis code). The AER and GSFC 2-D modeling teams have reached an agreement whereby AER will adopt the transport parameters of the GSFC model, and GSFC will adopt the diurnal chemical scheme of the AER model. As this paper helps to document the differences in the two models, it forms a bridge to the future model, which combines the best of both.

[49] **Acknowledgments.** This work was supported by the NASA Atmospheric Chemistry Modeling and Analysis Program and the NASA Atmospheric Effects of Aviation Project. Portions of this work were performed under the auspices of the U.S. Department of Energy by the University of California Lawrence Livermore National Laboratory under contract W-7405-Eng-48.

References

Anderson, D. E., Jr., and S. A. Lloyd (1990), Polar twilight UV-visible radiation field: Perturbations due to multiple scattering, ozone depletion, stratospheric clouds, and surface albedo, *J. Geophys. Res.*, *95*, 7429–7434.

Anderson, D. E., Jr., and R. R. Meier (1979), Effects of anisotropic multiple scattering on solar radiation in the troposphere and stratosphere, *Appl. Opt.*, *18*, 1955–1960.

Considine, D. B., A. R. Douglass, and C. H. Jackman (1994), Effects of a polar stratospheric cloud parameterization on ozone depletion due to stratospheric aircraft in a two-dimensional model, *J. Geophys. Res.*, *99*, 18,879–18,894.

Considine, D. B., A. R. Douglass, P. S. Connell, D. E. Kinnison, and D. A. Rotman (2000), A polar stratospheric cloud parameterization for the three dimensional model of the global modeling initiative and its response to stratospheric aircraft, *J. Geophys. Res.*, *105*, 3955–3975.

DeMore, W. B., et al. (1997), Chemical kinetics and photochemical data for use in stratospheric modeling, Evaluation number 12, *JPL Publ. 97-4*.

Dopplick, T. G. (1979), Radiative heating of the global atmosphere: Corrigendum, *J. Atmos., Sci.*, *36*, 1812–1817.

Douglass, A. R., M. P. Prather, T. M. Hall, S. E. Strahan, P. J. Rasch, L. C. Sparling, L. Coy, and J. M. Rodriguez (1999), Choosing meteorological input for the global modeling initiative assessment of high speed aircraft, *J. Geophys. Res.*, *104*, 27,545–27,564.

Fleming, E. L., S. Chandra, C. H. Jackman, D. B. Considine, and A. R. Douglass (1995), The middle atmospheric response to short and long term solar UV variations: Analysis of observations and 2D model results, *J. Atmos. Terr. Phys.*, *57*, 333–365.

Fleming, E. L., C. H. Jackman, R. S. Stolarski, and D. B. Considine (1999), Simulation of stratospheric tracers using an improved empirically based two-dimensional model transport formulation, *J. Geophys. Res.*, *104*, 23,911–23,934.

Garcia, R. R. (1991), Parameterization of planetary wave breaking in the middle atmosphere, *J. Atmos. Sci.*, *48*, 1405–1419.

Garcia, R. R., and S. Solomon (1983), A numerical model of the zonally averaged dynamical and chemical structure of the middle atmosphere, *J. Geophys. Res.*, *88*, 1379–1400.

Hall, T. M., D. W. Waugh, K. A. Boering, and R. A. Plumb (1999), Evaluation of transport in stratospheric models, *J. Geophys. Res.*, *104*, 18,815–18,839.

Holton, J. R., and X. Zhu (1984), A further study of gravity wave induced drag and diffusion in the mesosphere, *J. Atmos. Sci.*, *41*, 2653–2662.

Intergovernmental Panel on Climate Change (IPCC) (1999), *Aviation and the Global Atmosphere*, Cambridge Univ. Press, New York.

Jackman, C. H., A. R. Douglass, K. F. Brueske, and S. A. Klein (1991), The influence of dynamics on two-dimensional model results: Simulations of ^{14}C and stratospheric aircraft NO_x injections, *J. Geophys. Res.*, *96*, 22,559–22,572.

Jackman, C. H., E. L. Fleming, S. Chandra, D. B. Considine, and J. E. Rosenfield (1996), Past, present, and future modeled ozone trends with comparisons to observed trends, *J. Geophys. Res.*, *101*, 28,753–28,767.

Jacobson, M. Z. (1995), Computation of global photochemistry with SMVGEARII, *Atmos. Environ.*, *29*, 2541–2546.

Kalnay, E., et al. (1996), The NCEP/NCAR 40-year reanalysis project, *Bull. Am. Meteorol. Soc.*, *77*, 437–471.

Kawa, S. R., et al. (1999), Assessment of the effects of high-speed aircraft in the stratosphere: 1998, *Rep. NASA/TP-1999-209237*, Greenbelt, Md.

Kinnison, D. E., H. S. Johnston, and D. J. Wuebbles (1994a), Model study of atmospheric transport using carbon-14 and strontium-90 as inert tracers, *J. Geophys. Res.*, *99*, 20,647–20,664.

Kinnison, D. E., K. E. Grant, P. S. Connell, D. A. Rotman, and D. J. Wuebbles (1994b), Chemical and radiative effects of the Mount Pinatubo eruption, *J. Geophys. Res.*, *99*, 25,705–25,731.

Kinnison, D. E., et al. (2001), The Global Modeling Initiative assessment model: Application to high-speed civil transport perturbation, *J. Geophys. Res.*, *106*, 1693–1711.

Ko, M. K. W., K. K. Tung, D. K. Weisenstein, and N. D. Sze (1985), A zonal mean model of stratospheric tracer transport in isentropic coordinates: Numerical simulations for nitrous oxide and nitric acid, *J. Geophys. Res.*, *90*, 2313–2329.

Li, L., T. R. Nathan, and D. J. Wuebbles (1995), Topographically forced planetary wave breaking in the stratosphere, *Geophys. Res. Lett.*, *22*, 2953–2956.

Lin, S. J., and R. B. Rood (1996), Multidimensional flux-form semi-Lagrangian transport schemes, *Mon. Weather Rev.*, *124*, 2046–2070.

Lindzen, R. S. (1981), Turbulence and stress owing to gravity wave and tidal breakdown, *J. Geophys. Res.*, *86*, 9707–9714.

Minschwaner, K., G. P. Anderson, L. A. Hall, and K. Yoshino (1992), Polynomial coefficients for calculating O_2 Schumann-Runge cross sections at 0.5 cm^{-1} resolution, *J. Geophys. Res.*, *97*, 10,103–10,108.

Newell, R. E., J. W. Kidson, D. G. Vincent, and G. J. Boer (1974), *The General Circulations of the Tropical Atmosphere, vol. 2*, MIT Press, Cambridge, Mass.

Oort, A. H. (1983), Global atmospheric circulation statistics, 1958–1983, *NOAA Prof. Pap. 14*, Silver Spring, Md.

Park, J. H., M. K. W. Ko, C. H. Jackman, R. A. Plumb, J. A. Kaye, and K. H. Sage (1999), Models and measurements intercomparison II, *Rep. NASA/TM-1999-209554*, Greenbelt, Md.

Pitari, G. (1993), Contribution to the ozone trend of heterogeneous reactions of $ClONO_2$ on the sulfate aerosol layer, *Geophys. Res. Lett.*, *20*, 2663–2666.

Poole, L. R., and M. C. Pitts (1994), Polar stratospheric cloud climatology based on Stratospheric Aerosol Measurement II observation from 1978 to 1989, *J. Geophys. Res.*, *99*, 13,083–13,089.

Prather, M. J. (1993), I. GISS photochemical model in *The Atmospheric Effects of Stratospheric Aircraft: Report of the 1992 Models and Measurements Workshop*, NASA Ref. Publ. 1292, edited by M. J. Prather and E. E. Remsberg, pp. 76–85, Greenbelt, Md.

Prather, M. J., and E. E. Remsberg (Eds.) (1993), The atmospheric effects of stratospheric aircraft: Report of the 1992 Models and Measurements Workshop, NASA Ref. Publ. 1292, Greenbelt, Md.

Randel, W. J., and R. R. Garcia (1994), Application of a planetary wave breaking parameterization to stratospheric circulation statistics, *J. Atmos. Sci.*, *51*, 1157–1168.

Rosenfield, J. E., P. A. Newman, and M. R. Schoeberl (1994), Computations of diabatic descent in the stratospheric polar vortex, *J. Geophys. Res.*, *99*, 16,677–16,689.

Rossow, W. B., and R. A. Schiffer (1999), Advances in understanding clouds from ISCCP, *Bull. Am. Meteorol. Soc.*, *80*, 2261–2287.

Rotman, D. A., et al. (2001), The Global Modeling Initiative Assessment Model: Model description, integration and testing of the transport shell, *J. Geophys. Res.*, *106*, 1669–1691.

Sander, S. P., et al. (2000), Chemical kinetics and photochemical data for use in stratospheric modeling, Supplement to evaluation 12: Update of key reactions, Evaluation Number 13, *JPL Publ. 00-3*.

Shia, R.-L., M. K. W. Ko, D. K. Weisenstein, C. Scott, and J. Rodriguez (1998), Transport between the tropical and mid-latitude lower stratosphere: Implication for ozone response to HSCT emissions, *J. Geophys. Res.*, *103*, 25,435–25,446.

Smolarkiewicz, P. K. (1984), A simple positive definite advection scheme with small implicit diffusion, *Mon. Weather Rev.*, *111*, 479–487.

Stolarski, R. S., et al. (1995), Scientific assessment of the atmospheric effects of stratospheric aircraft, *NASA Ref. Publ. 1381*, Greenbelt, Md.

Weisenstein, D. K., M. K. W. Ko, I. G. Dyominov, G. Pitari, L. Ricciardulli, G. Visconti, and S. Bekki (1998), The effect of sulfur emissions from HSCT aircraft: A 2-D model intercomparison, *J. Geophys. Res.*, *103*, 1527–1547.

P. S. Connell, D. E. Kinnison, and D. A. Rotman, Lawrence Livermore National Laboratory, Livermore, CA 94550, USA. (connell2@llnl.gov; dkin@ucar.edu; rotman1@llnl.gov)

D. B. Considine, E. L. Fleming, and C. H. Jackman, NASA Goddard Space Flight Center, Greenbelt, MD 20771, USA. (david.b.considine@nasa.gov; fleming@kahuna.gsfc.nasa.gov; charles.h.jackman@nasa.gov)

J. Eluszkiewicz, M. K. W. Ko, C. J. Scott, and D. K. Weisenstein, Atmospheric and Environmental Research, Inc., 131 Hartwell Ave., Lexington, MA 02421, USA. (jel@aer.com; malcolm.k.ko@nasa.gov; scott@aer.com; dkweis@aer.com)